© 2022. Published by The Company of Biologists Ltd | Development (2022) 149, dev201203. doi:10.1242/dev.201203

RESEARCH ARTICLE

Plap-1 lineage tracing and single-cell transcriptomics reveal cellular dynamics in the periodontal ligament

Tomoaki Iwayama[1,‡,§], Mizuho Iwashita[1,‡], Kazuya Miyashita[2], Hiromi Sakashita[1,3], Shuji Matsumoto[1], Kiwako Tomita[1], Phan Bhongsatiern[1], Tomomi Kitayama[2,4], Kentaro Ikegami[2], Takashi Shimbo[3,4], Katsuto Tamai[4], Masanori A. Murayama[5,*], Shuhei Ogawa[5], Yoichiro Iwakura[5], Satoru Yamada[6], Lorin E. Olson[7], Masahide Takedachi[1] and Shinya Murakami[1,§]

ABSTRACT

Periodontal tissue supports teeth in the alveolar bone socket via fibrous attachment of the periodontal ligament (PDL). The PDL contains periodontal fibroblasts and stem/progenitor cells, collectively known as PDL cells (PDLCs), on top of osteoblasts and cementoblasts on the surface of alveolar bone and cementum, respectively. However, the characteristics and lineage hierarchy of each cell type remain poorly defined. This study identified periodontal ligament associated protein-1 (Plap-1) as a PDL-specific extracellular matrix protein. We generated knock-in mice expressing CreER^{T2} and GFP specifically in *Plap-1*-positive PDLCs. Genetic lineage tracing confirmed the long-standing hypothesis that PDLCs differentiate into osteoblasts and cementoblasts. A PDL single-cell atlas defined cementoblasts and osteoblasts as *Plap-1*$^{-}$*Ibsp*$^{+}$*Sparcl1*$^{+}$ and *Plap-1*$^{-}$*Ibsp*$^{+}$*Col11a2*$^{+}$, respectively. Other populations, such as *Nes*$^{+}$ mural cells, S100B^{+} Schwann cells, and other non-stromal cells, were also identified. RNA velocity analysis suggested that a *Plap-1*^{high}*Ly6a*$^{+}$ cell population was the source of PDLCs. Lineage tracing of *Plap-1*$^{+}$ PDLCs during periodontal injury showed periodontal tissue regeneration by PDLCs. Our study defines diverse cell populations in PDL and clarifies the role of PDLCs in periodontal tissue homeostasis and repair.

KEY WORDS: Periodontal tissue, Alveolar bone, Periodontal ligament, Extracellular matrix, Progenitor cell, Stem cell, Mural cell, Single-cell analysis, Cell atlas, Wound healing

INTRODUCTION

Mammalian teeth are supported by periodontal tissue, which consists of the periodontal ligament (PDL), gingiva, alveolar bone and cementum. As periodontal tissue is highly adaptive to normal and excess occlusal and orthodontic forces, it undergoes extensive remodeling (Beertsen et al., 1997). Periodontal tissue also possesses some regenerative capacity, as demonstrated in human and animal models (Sallum et al., 2019; Kitamura et al., 2016; Nagayasu-Tanaka et al., 2015). The plasticity of periodontal tissue is thought to be underpinned by the mesenchymal stem/progenitor population in the PDL (Zhao et al., 2020). This population presumably gives rise to three stromal lineages: periodontal fibroblasts, cementoblasts and osteoblasts (Luan et al., 2009; Iwayama et al., 2022). The PDL has also gained attention as a potent source of mesenchymal stem/stromal cells (MSCs) (Sharpe, 2016) or multipotent stromal cells (Soliman et al., 2021). The PDL contains various other cell types, including epithelial cell rests of Malassez (Xiong et al., 2013), hematopoietic cells (Wilson et al., 2018) and neurovascular cells (Men et al., 2020). However, evidence regarding the lineage characteristics and cellular hierarchies of the adult mammalian PDL *in vivo* remains limited.

One reason for this ambiguity is the lack of clear phenotypic markers that distinguish the PDL fibroblast lineage [periodontal ligament cells (PDLCs), including stem/progenitor cells and fibroblasts)] from other lineages of the periodontium. Based on recent lineage-tracing analyses, many mesenchymal stem/progenitor markers have been proposed, including GLI-Kruppel family member GLI1 (Gli1)-, alpha-smooth muscle actin (αSMA)- and Axin2-positive cells in the adult PDL (Roguljic et al., 2013; Yuan et al., 2018; Men et al., 2020). However, none of these markers is exclusively expressed in the PDL. Rather, they are also expressed in other components of the periodontium, as these markers are readouts of essential signaling pathways (sonic hedgehog, transforming growth factor β and Wnt signaling, respectively) with dynamic expression in various tissues. Another challenge in PDL biology is the lack of efficient methods for isolating cells from tissues. Owing to strong fiber attachments, dissociating the adult PDL is difficult (De Jong et al., 2017). Recent single-cell transcriptome analyses of the periodontium have revealed that isolated cells predominantly comprise epithelial cells (Caetano et al., 2021) and constitute only a small number of PDL-derived stromal cells (Krivanek et al., 2020; Pagella et al., 2021). In this regard, a method for isolation and evaluation is required to decipher the cellular hierarchy of the PDL.

The PDL expresses a large number of extracellular matrix (ECM) components, including collagen (Naveh et al., 2018) and proteoglycans (Chen et al., 2021). Among these, several genes are candidate PDL-specific genes (Takimoto et al., 2015; Horiuchi et al., 1999). We previously identified periodontal ligament associated protein-1 (*PLAP-1*; also known as *ASPN*) from a human cDNA library and demonstrated that it is highly expressed in the PDL at the transcript and protein levels (Yamada et al., 2001, 2007). PLAP-1 is a 43-kDa ECM protein that is a subtype of the small

[1]Department of Periodontology, Osaka University Graduate School of Dentistry, Suita, Osaka 565-0871, Japan. [2]StemRIM Inc., Ibaraki, Osaka 567-0085, Japan. [3]StemRIM Institute of Regeneration-Inducing Medicine, Osaka University, Suita 565-0871, Japan. [4]Department of Stem Cell Therapy Science, Osaka University Graduate School of Medicine, Osaka 565-0871, Japan. [5]Research Institute for Biomedical Sciences, Tokyo University of Science, Noda, Chiba 278-8510, Japan. [6]Department of Periodontology and Endodontology, Tohoku University Graduate School of Dentistry, Sendai, Miyagi 980-8575, Japan. [7]Cardiovascular Biology Research Program, Oklahoma Medical Research Foundation, Oklahoma City, OK 73104, USA.
*Present address: Department of Animal Models for Human Diseases, Institute of Biomedical Science, Kansai Medical University, Hirakata, Osaka 573-1191, Japan.
‡These authors contributed equally to this work

§Authors for correspondence (iwayama.tomoaki.dent@osaka-u.ac.jp; murakami.shinya.dent@osaka-u.ac.jp)

T.I., 0000-0002-3405-5822; M.A.M., 0000-0002-0049-0316; Y.I., 0000-0002-9934-5775; L.E.O., 0000-0003-2168-7836; M.T., 0000-0003-0331-3478; S. Murakami, 0000-0002-5230-452X

Handling Editor: James Briscoe
Received 9 August 2022; Accepted 5 September 2022

Development (2022) 149, dev201203. doi:10.1242/dev.201203

leucine-rich family of proteoglycans (SLRPs) (Kalamajski and Oldberg, 2010). PLAP-1 functions as a negative regulator of cytodifferentiation and mineralization of PDLCs through interactions with BMP2 and FGF2 (Yamada et al., 2006, Awata et al., 2005). Its transcript levels in the maxilla, including the PDL, have been reported to be more than tenfold greater than levels in adipose tissue, brain, heart, lung, liver, stomach, intestine, kidney, spleen, bone marrow and muscle (Sakashita et al., 2021). Compared with dissected gingiva, dissected PDLs contain 60 times more transcripts (Ueda et al., 2021). Nevertheless, the expression of *PLAP-1* in the PDL at the single-cell resolution has yet to be investigated.

In this study, we identified mouse *Plap-1* as a molecule that clearly distinguishes the PDL fibroblast lineage from other lineages, including osteoblasts and cementoblasts. Using knock-in mice expressing GFP and CreER^{T2} under the endogenous transcriptional control of *Plap-1*, we demonstrated that PDL cells differentiated into osteoblasts and cementoblasts *in vivo*. Furthermore, we developed a method for highly efficient isolation of PDL-derived cells based on GFP expression in knock-in mice. A single-cell transcriptome atlas of the PDL revealed its cellular heterogeneity including *Plap-1*$^{+}$*Nes*$^{+}$ mural cells, and Schwann cells and other non-stromal cells. Platelet-derived growth factor receptor alpha (PDGFRα)$^{+}$ stromal cells in PDL could be divided into *Plap-1*$^{+}$ PDLCs and bone sialoprotein (*Ibsp*)$^{+}$ cemento-/osteoblastic cells. Among *Ibsp*$^{+}$ cells, SPARC-like 1 (*Sparcl1*) and collagen type XI alpha 2 (*Col11a2)* were exclusively expressed in cementoblasts and osteoblasts, respectively. RNA velocity analysis suggested that *Plap-1*^{high}Ly6a (also known as Sca-1)$^{+}$ cells were the source of adult PDLCs. Upon tissue injury, PDLCs expanded to repair the periodontal tissue. These results advance our understanding of the PDL and its mechanisms of regeneration in both healthy and diseased states.

RESULTS

Identification of *Plap-1* as a PDLC-specific marker

The PDL is the ECM-rich connective tissue between the cementum and alveolar bone. Histological staining of this tissue revealed spindle-shaped fibroblastic cells aligned along the horizontal axis of the fiber bundles (Fig. 1A). To identify exact cell types according to gene expression profiles at single-cell resolution, we performed fluorescence *in situ* hybridization (FISH). We confirmed that both lineages expressed ECM components, such as collagen type I alpha 1 (*Col1a1*), biglycan (*Bgn*) and secreted protein acidic and rich in cysteine (*Sparc*) (Fig. 1B,C, Fig. S1A). Cementoblasts and osteoblasts were labeled with secreted phosphoprotein 1 (*Spp1*) and *Ibsp* (Fig. 1D,F) as previously reported (Foster et al., 2018). We then found that only fibroblast-like cells in the PDL in the horizontal direction were positive for *Plap-1*, whereas the layer of cells on the surface of the alveolar bone and cementum was negative for *Plap-1* (Fig. 1E). FISH using both *Plap-1* and *Ibsp* probes showed that these cells are mutually exclusive in PDL (Fig. 1F). As Plap-1 is a secreted protein, its protein distribution was widespread throughout the PDL and could be seen around osteoblasts and cementoblasts in addition to the Plap-1-producing PDLCs (Fig. 1E versus Fig. S1B). Having identified *Plap-1* as a molecular marker that specifically labels the periodontal fibroblast lineage (including stem/progenitor cells), we defined the three previously proposed zones of the PDL (Lee et al., 2015) using *Plap-1* and *Ibsp* (Fig. 1G).

Generation of PDLC-specific knock-in mice and lineage tracing

Next, we devised a strategy for CreER-2A-GFP knock-in to faithfully reproduce *Plap-1* expression in mice (Fig. S1C-F). GFP expression in *Plap-1-GFP-2A-CreER* mice was consistent with the FISH results, and only cells in the fibroblastic zones were labeled (Fig. 2A). Furthermore, using the tamoxifen-induced Cre expression system, genetic lineage tracing of *Plap-1*$^{+}$ cells can be conducted with the knock-in mice (Fig. 2B). Short-term lineage tracing revealed that they were restricted to the fibroblastic zone 2 days after treatment with tamoxifen (Fig. 2C), as expected. The tight regulation of CreER was further confirmed by the absence of tdTomato expression without tamoxifen treatment (Fig. S1G) and limited tdTomato expression by a lower (one-tenth) dose tamoxifen treatment (Fig. S1H). The PDLCs were traced for a further 3 months, when fibroblastic turnover of the tissue was completed (Sodek, 1977). The PDL still consisted of tdTomato^{+} cells, suggesting that the PDL homeostasis was maintained by *Plap-1*$^{+}$ stem/progenitor cells (Fig. 2D). TdTomato^{+} cells were also observed both in cemento-/osteoblastic zones at 3 months post-treatment (Fig. 2D), suggesting that *Plap-1*$^{+}$ cells gave rise to cemento-/osteoblast lineage cells. This was also confirmed by the existence of *Ibsp*-expressing PDLC lineage cells in the middle and furcation areas of PDL (Fig. 2E). In addition, we investigated Plap-1 expression in other tissues using the knock-in mice (Fig. S2A-L) and confirmed the specificity of Plap-1 expression in the PDL as previously reported (Sakashita et al., 2021).

Development of a protocol for isolation of PDL-derived cells

To decipher the cell types in the PDL that contribute to the homeostasis and repair of periodontal tissue, an efficient method for isolation and analysis of PDL cells is required. We previously established a method for isolating PDL-derived cells by scraping the root surface with a PDL explant (Ueda et al., 2021). However, this method can only be used to analyze migratory cells. In this study, we used GFP expression in *Plap-1-GFP-2A-CreER* mice to evaluate the efficacy of PDL cell isolation. We adopted our previous protocol in which the gingiva was removed from the maxilla before tooth extraction to avoid any contamination from the gingival cells to extracted molars (Ueda et al., 2021). We first digested the scraped PDL with enzymes. Nevertheless, we did not observe any clear cell populations in the forward scatter (FSC)/side scatter (SSC) plot (Fig. S3A). We then modified the protocol to digest extracted whole teeth (Fig. 3A) and observed a clear population in the FSC/SSC plot (Fig. S3A). Using flow cytometry and microscopy, we compared two enzymes, Liberase and Collagenase II. We identified a more evident population in the FSC/SSC plot with the use of Liberase (Fig. S3B). This was in agreement with the observation that the PDL was completely removed from the root surface with the use of Liberase (Fig. S3C). Histological analysis of the alveolar socket after tooth extraction showed that PDL tissue remained on the alveolar bone surface, but cells in the furcation area close to the alveolar crest were mostly removed (Fig. S3D). We further confirmed that Liberase treatment was superior in terms of the percentage and the absolute number of live cells (Fig. S3E). Efficient PDL detachment from the tooth surface with Liberase was confirmed histologically (Fig. 3B). The isolated cells were analyzed using flow cytometry, and a gating strategy was established according to GFP expression. GFP^{+} cells from live singlets were backgated onto the FSC/SSC plot, and the gating was defined as a PDL-enriched population (Fig. 3C). This population was then used to determine the relative proportion of each cell type. PDL cell-enriched populations yielded more than 10,000 cells per animal, of which 20%, 6% and 10% comprised CD45 (Ptprc)$^{+}$ immune cells, CD31 (Pecam1)$^{+}$ vascular endothelial cells and CD326 (Epcam)$^{+}$ epithelial cells, respectively (Fig. 3D).

Development (2022) 149, dev201203. doi:10.1242/dev.201203

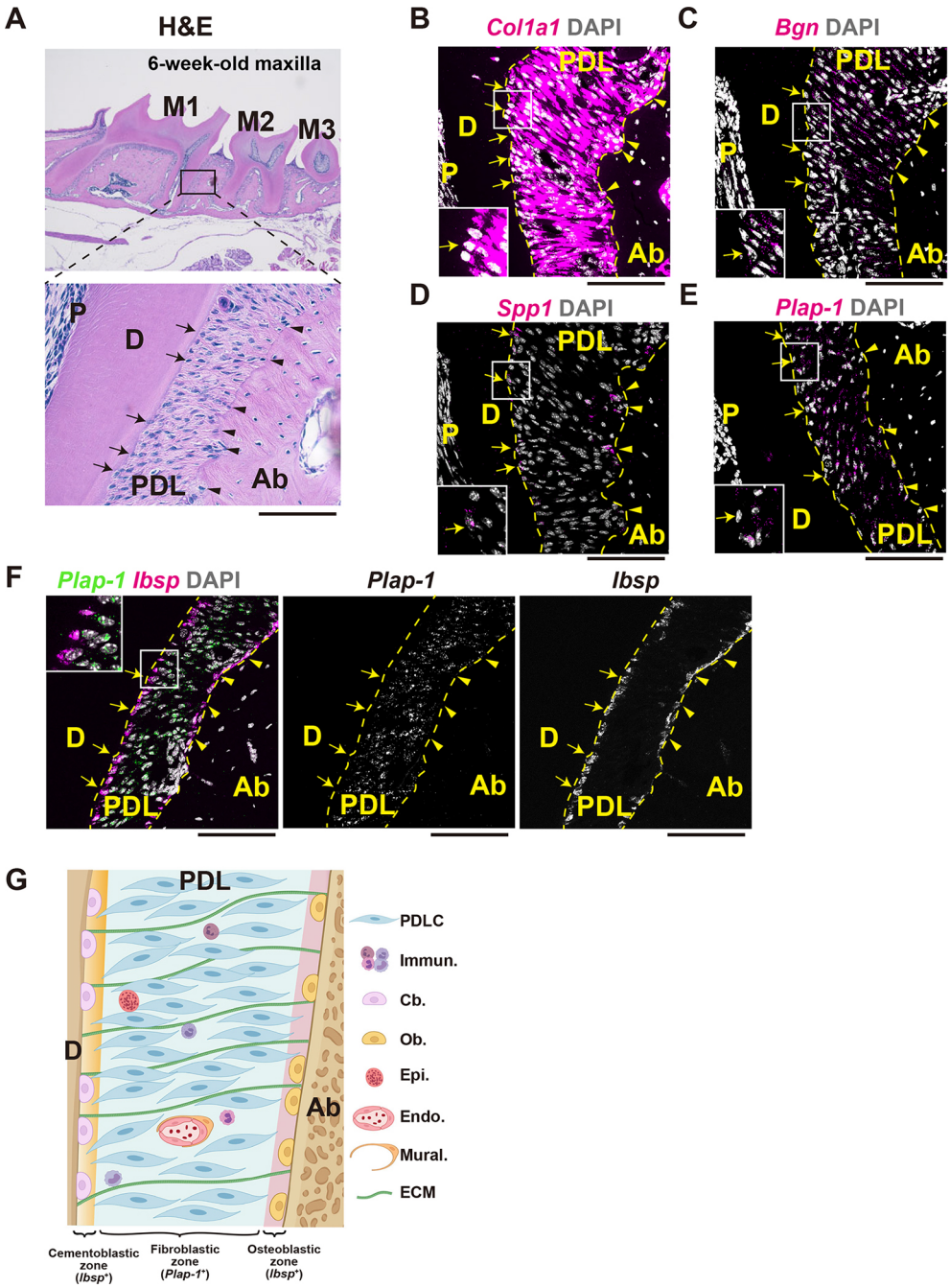

Fig. 1. Fibroblastic and cemento-/osteoblastic zones in the PDL. (A) Representative HE staining of 6-week-old wild-type maxilla (lower magnification in upper panel) and the PDL (higher magnification in lower panel). Arrows indicate cementoblasts. Arrowheads indicate osteoblasts. PDL images in all figures are presented in this direction (left: cementum/dentin/root; right: alveolar bone). (B) Representative *Col1a1* mRNA expression in the PDL. Most cells in the PDL, including cemento-/osteoblasts, expressed *Col1a1*. (C) Representative *Bgn* mRNA expression in the PDL. Similar to *Col1a1*, most cells in the PDL, including cemento-/osteoblasts, expressed *Bgn*. (D) Representative *Spp1* mRNA expression in the PDL. *Spp1* was expressed only in cells on the surface of the alveolar bone and cementum. (E) Representative *Plap-1* mRNA expression in the PDL. In contrast to *Spp1*, *Plap-1* was expressed in most cells in the PDL, but not in a subset of cells on the surface of the alveolar bone and cementum. (F) Representative *Plap-1* (green) and *Ibsp* (magenta) mRNA expression in the PDL. The expression of *Plap-1* and *Ibsp* was mutually exclusive. In B-F, insets show higher magnifications of the boxed areas. Dashed lines outline the PDL. Arrows and arrowheads indicate cementoblasts and osteoblasts, respectively. (G) Schematic of cellular composition in three zones of the PDL. The central part in the cementum-alveolar bone direction is designated as the *Plap-1*$^{+}$ fibroblastic zone. Either end (i.e. the surface of the cementum or alveolar bone) is designated as the *Ibsp*$^{+}$ cementoblastic or osteoblastic zone. Ab, alveolar bone; Cb., cementoblasts; D, dentin; Epi., epithelial rests of Malassez; Endo., endothelial cells; Immun., immune cells; M1, maxillary first molar; M2, maxillary second molar; M3, maxillary third molar; Mural., mural cells; P, pulp; Ob., osteoblasts. Experiments shown were conducted in 8- to 12-week-old mice unless otherwise specified. Scale bars: 100 µm.

In addition, we investigated whether a stromal cell marker, CD51, also known as integrin αV, can label stromal cells, including Plap-1^{+} cells. CD51^{+} cells included most GFP^{+} cells, with an average of 30% single-positive cells. GFP^{+} cells consistently accounted for approximately 30% of the population. We also tested the workflow using a Col1a1-GFP mouse line that expresses GFP in both

Development (2022) 149, dev201203. doi:10.1242/dev.201203

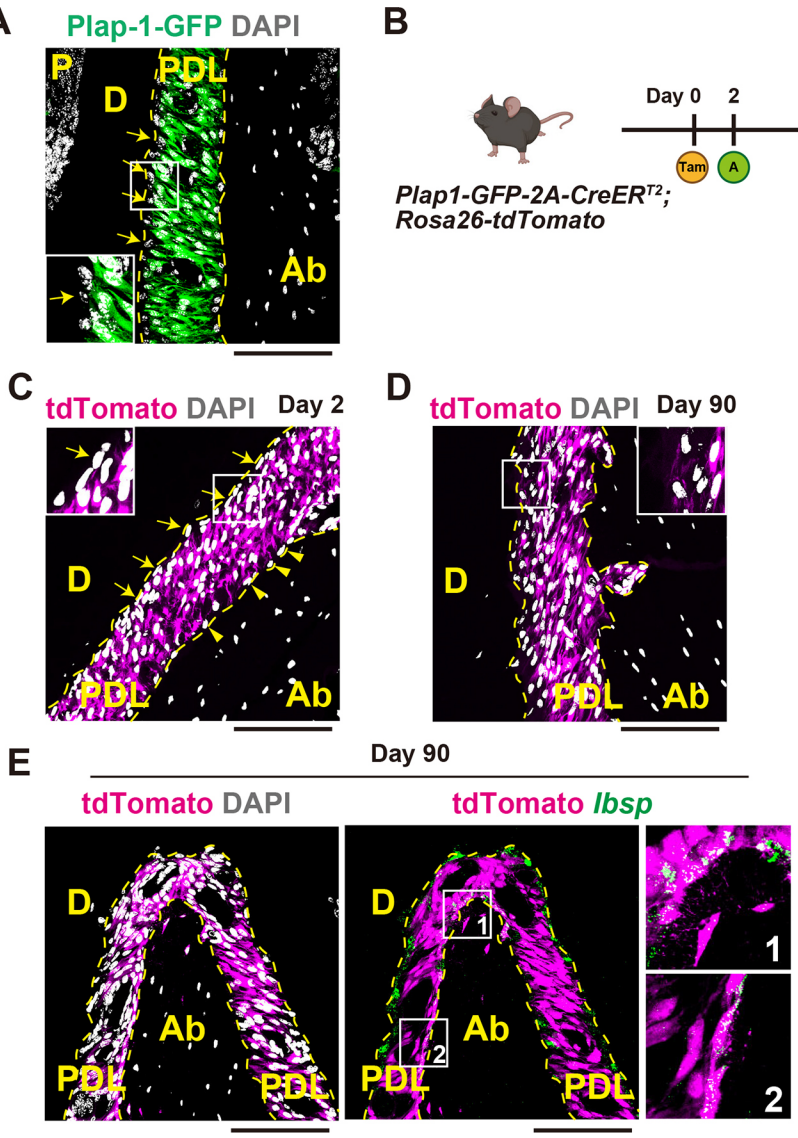

Fig. 2. *Plap-1*$^{+}$ cells maintain periodontal tissue. (A) Representative GFP expression in the PDL of *Plap-1-GFP-2A-CreER* knock-in mice. GFP expression was restricted to the fibroblastic zone. (B) Overview of the tamoxifen-induced lineage-tracing experiment. *Plap-1-GFP-2A-CreER; Rosa26-tdTomato* mice were generated, and tamoxifen was administered. In the system, a fusion protein of a mutated estrogen receptor and Cre recombinase is expressed in Plap-1^{+} cells, and the Plap-1^{+} cells are labeled with tdTomato once tamoxifen is administered. The mark is heritable and permanent and thus transmitted to all the descendants of Plap-1^{+} cells. A, analysis of the mice; Tam, single tamoxifen administration via intraperitoneal injection. (C) Representative tdTomato expression in the PDL 2 days after tamoxifen treatment. *Plap-1* lineage cells were restricted to the fibroblastic zone. (D) Representative tdTomato expression in the PDL 90 days after tamoxifen treatment. Cells in cemento-/osteoblastic zones were also positive for tdTomato. (E) Representative tdTomato (magenta) and *Ibsp* mRNA (green) expression in the PDL of the furcation area 90 days after tamoxifen treatment. Cells in cemento-/osteoblastic zones and some osteocytes were also double-positive for tdTomato and *Ibsp*. Insets show *Ibsp*-expressing Plap-1-lineage cells in higher magnifications of the boxed areas. Dashed lines outline the PDL. Arrows and arrowheads indicate cementoblasts and osteoblasts, respectively. Ab, alveolar bone; D, dentin; P, pulp. Scale bars: 100 µm.

fibroblastic and cemento-/osteoblastic cells in periodontal tissue (Fig. S3F). As expected, more GFP^{+} cells were observed in the Col1a1-GFP PDL than in the Plap-1-GFP PDL (Fig. S3G). A comparison of gingiva with the PDL revealed that Col1a1-GFP expression levels were higher in the PDL than in gingiva, consistent with a previous report that collagen turnover is more active in the PDL than in gingiva (Sodek, 1977). Additionally, we examined the culture conditions suitable for PDLCs and developed a method that enabled stable PDL cell expansion *in vitro* under hypoxic conditions (Fig. 3E). GFP^{+} cells exhibited significantly higher fibroblast colony-forming unit (CFU-F) formation compared with all cells from the PDL-enriched population (Fig. 3F) and demonstrated osteogenic differentiation capacity *in vitro* (Fig. 3G), confirming that PDLCs contain stem/progenitor cells. However, the cellular composition and heterogeneity of the PDL were not determined from this analysis.

Generation of a PDL atlas using single-cell transcriptome analysis

After establishing an efficient PDLC isolation technique, we obtained cell suspensions from 20 adult wild-type mice. All viable cells in the PDL were collected by cell sorting and subjected to single-cell transcriptome analysis to generate a 'PDL single-cell atlas' (Fig. 4A, B, Fig. S4A). After the removal of low-quality cells, 17 clusters were identified from the PDL single-cell RNA-sequencing (scRNA-seq) data (7318 cells) (Fig. 4C). The cell types in each cluster were annotated using known cell marker genes (Fig. 4D). The most abundant populations were stromal cells expressing collagens, matrix metalloproteinases and platelet-derived growth factor receptors (Fig. 4D, Fig. S4B). Consistent with the histological analysis (Fig. 1F), collagen-expressing stromal cells were mutually exclusively defined by the expression of *Plap-1* or *Ibsp* (Fig. 4E). The stromal cell cluster was subjected to in-depth analysis (Fig. 5). Non-stromal cell clusters, including immune, epithelial and vascular endothelial cells, were also identified (Fig. 4D, Fig. S4C, E). Flow cytometry analysis of isolated immune cells from PDL showed the presence of macrophages, proerythroblasts, B cells and T cells in the PDL and no overlap with Plap-1-GFP^{+} cells (Fig. S4D). Two epithelial cell clusters were distinguished by differential expression of keratin 15 (*Krt15*) and keratin 17 (*Krt17*). FISH analysis confirmed that *Krt17*-positive epithelial cells were derived from the inner and outer epithelia, whereas *Krt15*-positive epithelial cells were derived from the basement membrane (Fig. S4F). Notably, a cluster of *Plap-1*$^{+}$ cells exhibited distinct

Development (2022) 149, dev201203. doi:10.1242/dev.201203

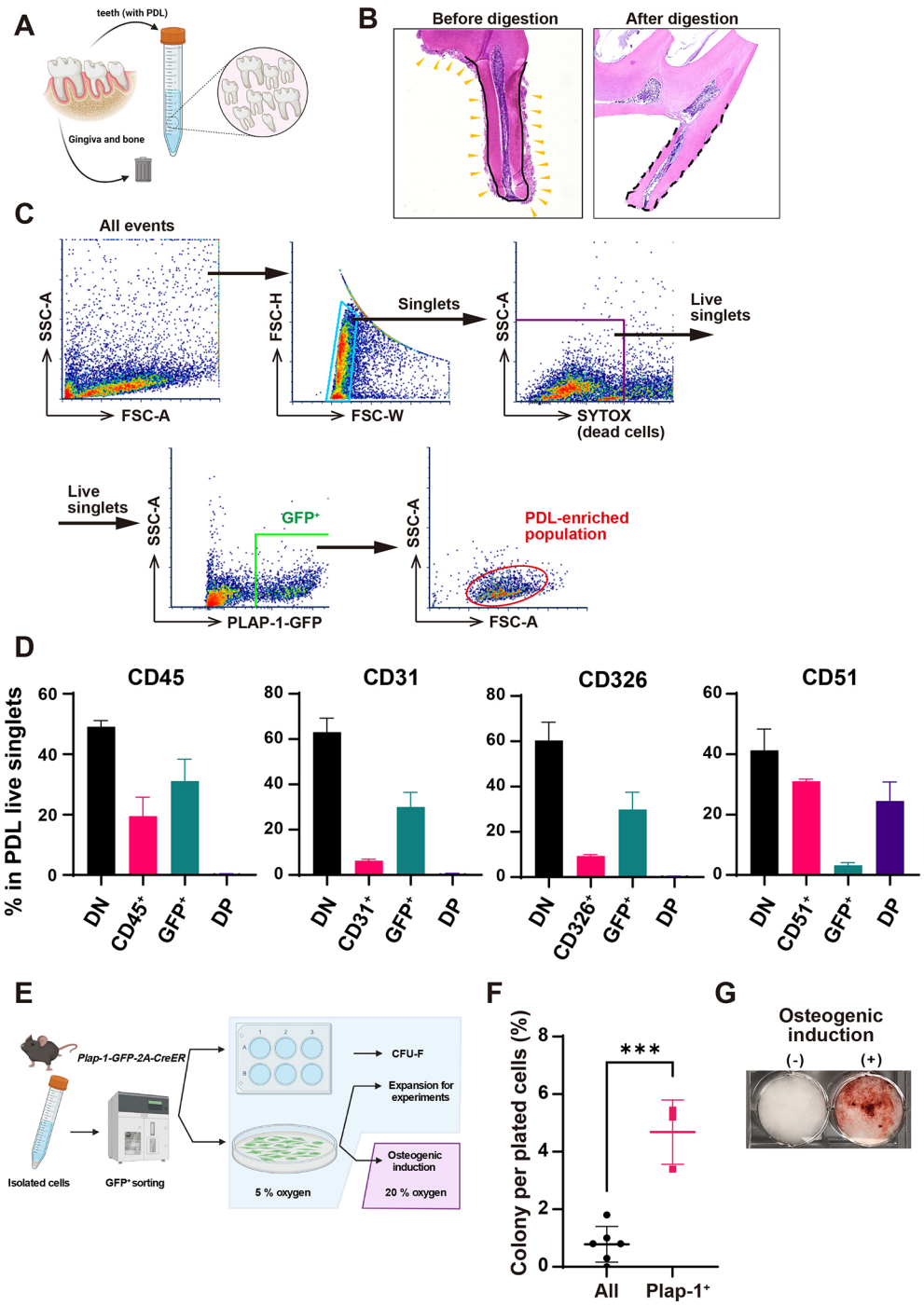

Fig. 3. Efficient isolation and culture of PDL cells. (A) Overview of cell isolation experiments. After cardiac perfusion with PBS, the maxillae and mandibles were dissected, and gingival tissue was carefully removed under a stereomicroscope. The teeth were extracted from the remaining maxillae and mandibles and subjected to further processing. (B) Representative HE staining of extracted teeth before and after Liberase digestion. The yellow arrowheads indicate PDL tissue in the left panel. In contrast, PDL tissue is absent but intact pulpal tissue is evident in the right panel. Solid line shows the outline of the root before enzyme treatment; dashed line shows the outline of the root after enzyme treatment. (C) A gating strategy for PDLC-enriched populations by flow cytometry. Several populations were observed in FSC-A/SSC-A plots. Within live singlets, GFP$^+$ PDLC was enriched in the green-colored gate shown in the FSC-A/SSC-A plot. (D) Cellular composition analysis by flow cytometry. Within the PDL-enriched population, CD45-, CD31-, CD326- and CD51-positive cells were quantified (n=3 mice). Error bars represent s.e.m. DN, double negative; DP, double positive. (E) Overview of cell culture experiments. After isolation of PDL-derived cells from wild-type or *Plap-1-GFP-2A-CreER* mice, single-cell suspensions were subjected to cell sorting using an SH800 cell sorter. Sorted cells were expanded or analyzed using a CFU-F assay under hypoxia, followed by osteogenic induction experiments in normoxic conditions. (F) CFU-F quantification. Plap-1-GFP$^+$ cells and PDL-enriched populations were compared. The difference was statistically significant (***P<0.001, two-tailed, unpaired t-test; n=3-6 mice; mean±s.d.). (G) Representative Alizarin Red S staining images. After 20 days of induction, calcified nodules were observed only in the induction group (+). Experiments were conducted in 8- to 12-week-old mice.

gene expression in stromal cell clusters. This cluster expressed *Nes*, regulator of G-protein signaling 5 (*Rgs5*) and myosin 11 (*Myh11*) (Fig. 4E,F), which are markers of vascular mural cells (vascular smooth muscle cells and pericytes), suggesting that the PDL also contains mural cell populations that are less heterogeneous than the fibroblast lineage (Muhl et al., 2020). To identify *Plap-1*$^+$*Nes*$^+$ cell clusters in PDL histology, we used *Nes-GFP* transgenic mice, in which stem/progenitor populations are labeled in other tissues (Méndez-Ferrer et al., 2010; Iwayama et al., 2015). Nes-GFP$^+$ cells exhibited a perivascular appearance, with long cellular processes along the blood vessels in the PDL (Fig. 4G). The cell bodies were covered by the basement membrane of vascular endothelial cells, suggestive of pericytes (Fig. 4H).

Cellular hierarchy of the PDL according to RNA velocity analysis

To identify the heterogeneity in the PDL that maintains tissue homeostasis, 3675 stromal cells expressing collagens, matrix metalloproteinases and platelet-derived growth factor receptors (Fig. S4B) were subjected to subclustering analysis. We identified 11 clusters (Fig. 5A) and confirmed that they were expressed either *Plap-1* or *Ibsp*, except cluster 8 (Fig. 5B). Intriguingly, *Scx*, *Mkx* and *Tnmd*, which have been previously reported to be PDLC specific, were expressed only in a subset of both *Plap-1*$^+$ and *Ibsp*$^+$ cells (Fig. S5A). It should be noted that the master regulators of osteogenic differentiation, Runt-related transcription factor 2 (*Runx2*) and Sp7 transcription factor 7 (*Sp7*, also known as

Development (2022) 149, dev201203. doi:10.1242/dev.201203

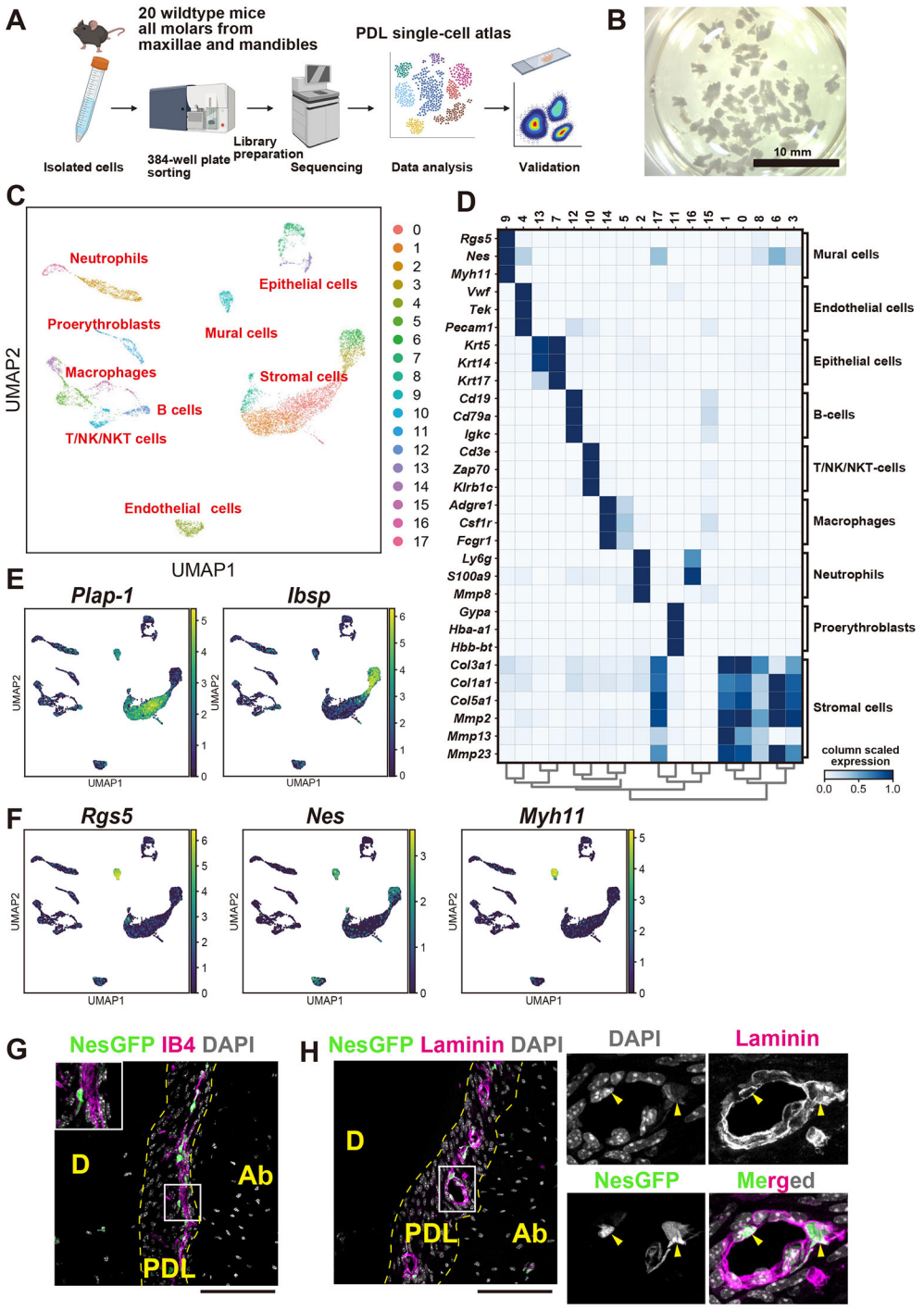

Fig. 4. Single-cell transcriptomic analysis of PDL-derived cells. (A) Overview of the experimental workflow. Teeth from 20 wild-type mice were subjected to cell isolation, and each cell type was sorted into 384 well plates with a lysis solution. Each lysate was then processed for library preparation, followed by sequencing and bioinformatic analysis. The identified molecules were validated using flow cytometry or histological analysis. (B) Representative photograph of extracted teeth used for scRNA-seq analysis. All molars were extracted from dissected maxillae and mandibles. (C) scRNA-seq data obtained from 7318 PDL-derived cells. Clustering analysis with 17 cell types is shown in UMAP. (D) A heatmap of the expression of representative genes for each cluster. Each cell type was annotated using these marker genes. (E) UMAP plots showing *Plap-1* and *Ibsp* expression. The expression of *Plap-1* and *Ibsp* was mutually exclusive. (F) UMAP plots showing *Rgs5*, *Nes* and *Myh11* expression. The expressions of *Rgs5*, *Nes* and *Myh11* were restricted to the mural cell cluster. (G) Representative GFP expression and GS-IB-4 staining in the PDL of Nestin-GFP mice. Insets showed Nestin-GFP$^+$ cells located in the perivascular area in the PDL. Inset shows a magnified view of the boxed area. (H) Representative laminin immunofluorescence staining in the PDL of Nestin-GFP mice. Nestin-GFP$^+$ cell bodies were encapsulated by the endothelial basement membrane. Magnified views of the boxed area are shown to the right. Arrowheads indicate Nestin-GFP$^+$ cells. Dashed lines in G,H delineate the PDL. Experiments shown in G,H were conducted in 8- to 12-week-old mice. Ab, alveolar bone; D, dentin. Scale bars: 10 mm (B); 100 µm (G,H).

osterix), were also globally expressed in both lineages, suggesting that PDLCs are readily differentiated into osteoblasts and cementoblasts (Fig. S5B). This skewed differentiation is also supported by the expression of other bone-related proteins and SLRPs in PDLCs (Fig. 1B,C, Fig. S1A). Based on the representative gene expression profile (Fig. 5C), cluster 8 was annotated as Schwann cells, and S100 calcium-binding protein B (S100B)-expressing cells were identified in the PDL (Fig. S5C). In addition to the annotation of each cell type within stromal cells, we conducted RNA velocity analysis, which can predict the future state of individual cells by distinguishing between unspliced and spliced mRNA (Fig. 5D). The results suggested that the cells in cluster 9 are the source of differentiated cells in the PDL environment. This cluster showed higher expression and positive velocity of *Plap-1* (Fig. S5D). In search of marker genes, lymphocyte activation protein 6a (*Ly6a*) and leucine rich repeat containing 15 (*Lrrc15*) were identified. The protein product of *Ly6a*, also known as stem cell antigen (Sca-1), has been used for identifying stem cells in many tissues in combination with another antigen, such as PDGFRα (Houlihan et al., 2012). The relative expression level of the *Ly6a* was higher in cluster 9 than in any other cluster (Fig. 5E), and we further characterized the population as Ly6a-positive *Plap-1*^{high} cells. Histological analysis revealed that they were located in the apical part of the PDL (Fig. 5F), and flow cytometry analysis showed they were 5.4% of the PDL live singlets (Fig. S5E). *Lepr*-, *Gli1*-, *Axin2*- *and Acta2*-positive cells have been implicated in stem/

Development (2022) 149, dev201203. doi:10.1242/dev.201203

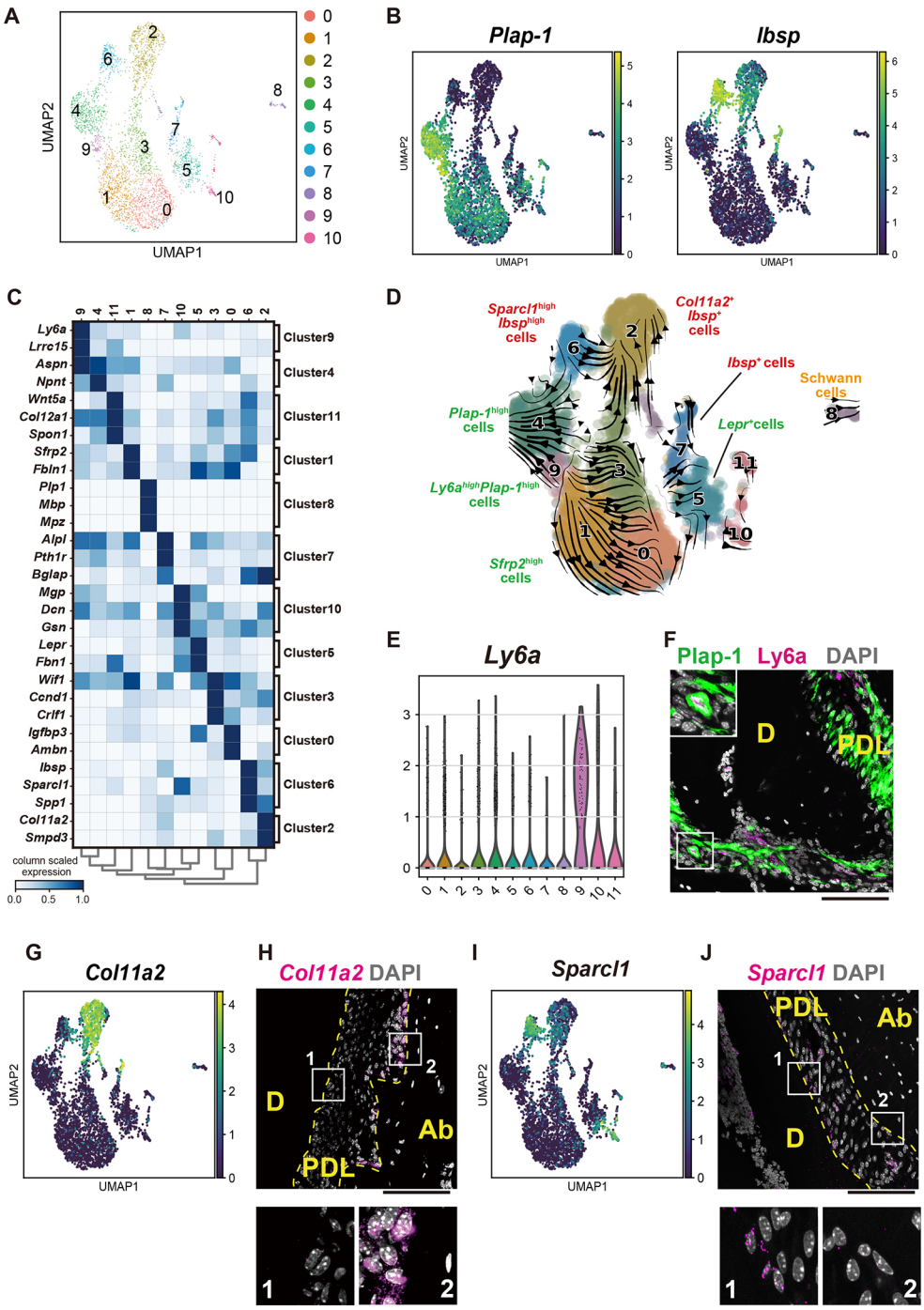

Fig. 5. Sub-clustering analysis of PDL stromal cells. (A) Sub-clustering analysis of stromal cells. (B) UMAP plots showing *Plap-1* and *Ibsp* expression. The expression of *Plap-1* and *Ibsp* was mutually exclusive. (C) A heatmap for representative genes for each cluster. (D) RNA velocity analysis of the sub-cluster. RNA velocity in every single cell was estimated by distinguishing between unspliced and spliced mRNAs, the balance of which is predictive of cellular state progression. Arrowed lines indicate direction of cellular state changes inferred by RNA velocity analysis. (E) Violin plot showing *Ly6a* expression in each cluster. The expression was specifically high in cluster 9. (F) Representative Ly6a immunofluorescence staining in the PDL. Ly6a^{+} PDL cells were located in the apical area of the PDL (inset; magnification of the boxed area). (G) *Col11a2* expression overlayed on a UMAP plot. The expression was specifically high in cluster 2. (H) Representative *Col11a2* mRNA expression in the PDL. The expression was restricted to the osteoblastic zone. (I) *Sparcl1* expression overlayed on UMAP plot. The expression was specifically high in cluster 6. (J) Representative *Sparcl1* mRNA expression in the PDL. The expression was restricted to the cementoblastic zone. In F,H,J, boxed areas are magnified below, as indicated. Experiments shown in H-J were conducted in 8- to 12-week-old mice. Ab, alveolar bone; D, dentin. Scale bars: 100 µm.

progenitor cells in the PDL. However, in this dataset, they were not associated with a specific cluster, with the exception of *Lepr*$^{+}$ cells, which were enriched in cluster 5 (Fig. S5F). Crucially, none of these cells were observed at the top of the lineage hierarchy (Fig. 5D). Among *Ibsp*$^{+}$ clusters, *Col11a2* expression was specific to cluster 2 (Fig. 5G), and this gene was exclusively expressed in osteoblasts but not in cementoblasts (Fig. 5H). Compared with the osteoblast cluster, the other *Ibsp*$^{+}$ cluster (cluster 6) expressed higher levels of *Sparcl1* (Fig. 5I). *Sparcl1* expression was observed in cementoblasts and cementocytes, but not in osteoblasts (Fig. 5J, Fig. S5G). However, the cluster did not specifically express recently reported markers (Nagata et al., 2021), including parathyroid hormone-related protein (*Pthlh*), class III β-tubulin (*Tubb3*) and Wnt inhibitory factor 1 (*Wif1*) (Fig. S5H). To assess the putative differentiation pathways, we also performed a pseudotime analysis of clusters 0, 2, 4 and 6. Gene expression kinetics of *Plap-1*, *Ibsp*, *Col3a1*, *Col1a1*, *Sparcl1*, *Col11a2*, *Lrrc15* and *Ly6a* showed unique transient changes during differentiation (Fig. S6A-F).

Plap-1^{+} PDLCs directly contribute to periodontal tissue repair

To investigate the role of PDLCs in the repair of injured periodontal tissue, we utilized a ligature-induced periodontitis model (Fig. 6A). In this widely used model (Abe and Hajishengallis, 2013), a suture is placed around the second molar of the maxilla for 7 days to induce periodontal tissue loss. Upon ligature removal, the periodontal

Development (2022) 149, dev201203. doi:10.1242/dev.201203

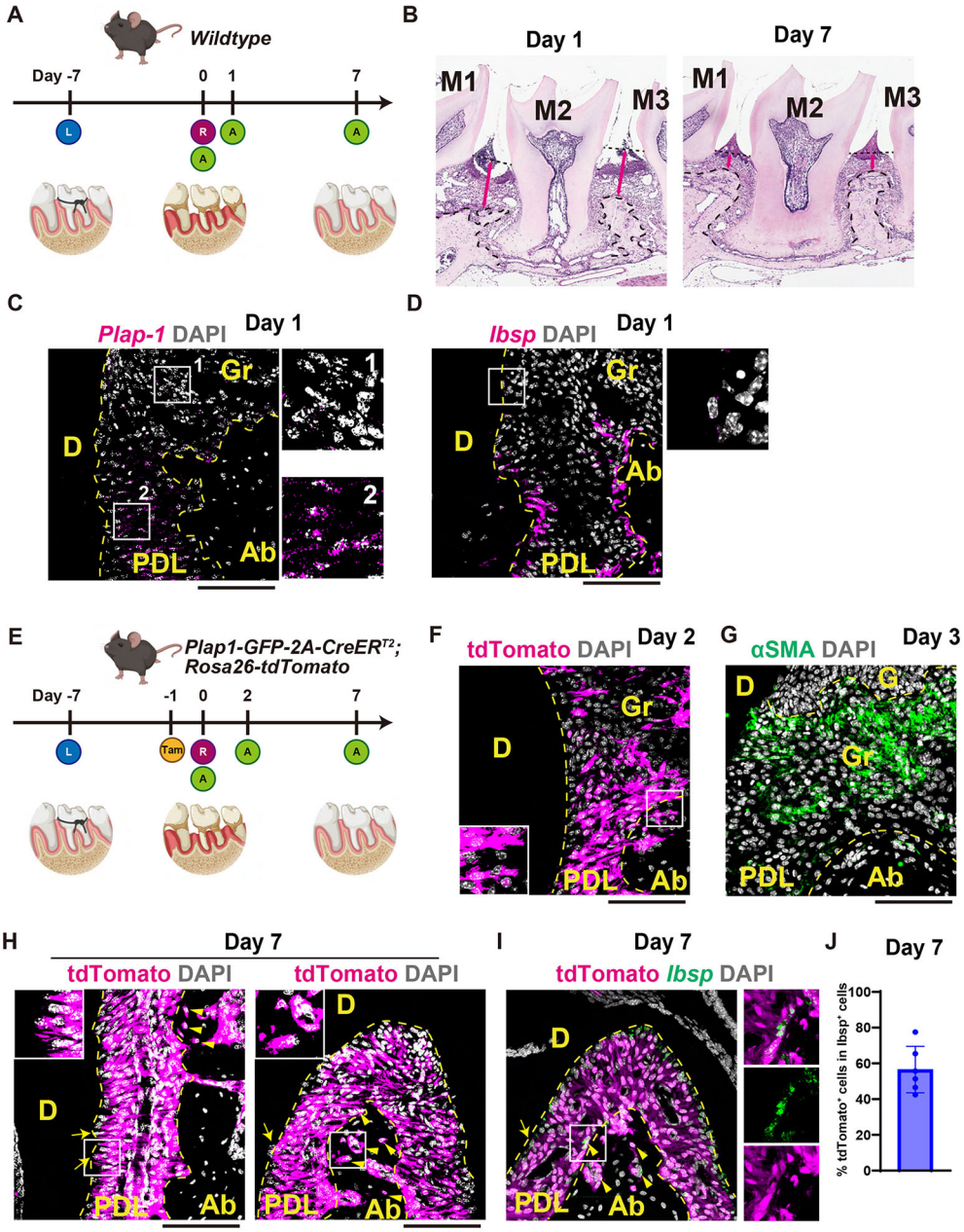

Fig. 6. *Plap-1* lineage cells in repaired periodontal tissue. (A) Overview of ligature-induced periodontitis experiments. Eight-week-old wild-type mice underwent ligature placement around the second molar of the maxilla. After 7 days, periodontal tissue was inflamed and destroyed. A week after suture removal, periodontal tissue was repaired. A, analysis of the mice; L, ligature placement; R; removal of suture. (B) Representative HE staining of periodontal tissue destruction. On the day of suture removal (day 0), the periodontal tissue was destroyed. The tissue consisted of newly formed granulation tissue and remaining periodontal tissue. Arrows show the distance between the cemento-enamel junction and the alveolar bone crest. Dashed line shows the cemento-enamel junction and the alveolar bone crest. (C) Representative *Plap-1* mRNA expression in the border of the remaining PDL and granulation tissue. Only the remaining PDL (defined by the presence of neighboring bone and cementum) expressed *Plap-1*. (D) Representative *Ibsp* mRNA expression in the border of the remaining PDL and granulation tissue. *Ibsp*$^{+}$ cementoblasts on the cementum surface were not evident beyond the border of the remaining PDL and granulation tissue. In C,D, boxed areas are magnified on the right, as indicated. (E) Overview of ligature-induced periodontitis experiments. *Plap-1-GFP-2A-CreER; Rosa26-tdTomato* mice were administered tamoxifen and underwent ligature placement around the second molar of the maxilla. The suture was removed 7 days after ligature placement (designated as day 0). The repair process was analyzed on days 2 and 7. A week after suture removal, periodontal tissue was repaired. A, analysis of the mice; L, ligature placement; R, removal of suture. (F) Representative tdTomato expression in repairing periodontal tissue 2 days after suture removal. Plap-1 lineage cells were distributed in granulation tissue. (G) Representative αSMA immunofluorescence staining in the granulation tissue 2 days after suture removal. αSMA^{+} cells were distributed in granulation tissue, but only 20.2% were derived from Plap-1 lineage cells based on quantification within histological sections (not shown). (H) Representative tdTomato expression in repairing periodontal tissue 7 days after suture removal. The repaired tissue consisted of *Plap-1* lineage cells. Of note, the osteocytes were differentiated from PDLCs (arrowheads). Insets show magnifications of the boxed areas. (I) Representative tdTomato (magenta) and *Ibsp* mRNA (green) expression in the PDL of the furcation area 7 days after suture removal. Some cells were double positive for tdTomato and *Ibsp* (highlighted with arrows for cementoblasts and arrowheads for osteoblasts). Insets show *Ibsp*-expressing Plap-1 lineage cells. Boxed area is shown at higher magnification to the right. (J) Quantification of tdTomato^{+} cells in *Ibsp*-expressing cells within histological sections. Mean±s.d. Ab, alveolar bone; D, dentin; Gr, granulation tissue. Dashed lines delineate the PDL. Scale bars: 100 µm.

Development (2022) 149, dev201203. doi:10.1242/dev.201203

tissue can be repaired to the baseline level 7-14 days after removal. On day 1, after ligature removal, a layer of cementum on the surface remained intact, although alveolar bone resorption was observed (Fig. 6B, left). On day 7, recovered alveolar bone levels and fibrous attachment between the bone and cementum were observed (Fig. 6B, right). *Plap-1* mRNA expression was restricted to the fibroblastic zone between the remaining alveolar bone and cementum (Fig. 6C), which was defined as the PDL. Notably, *Ibsp* expression was dramatically downregulated in the remaining cementum (Fig. 6D). To elucidate the contribution of *Plap-1*$^+$ cells in the remaining PDL to tissue repair, *Plap-1-GFP-2A-CreER; Rosa26-tdTomato* mice were administered tamoxifen 1 day before ligature removal (Fig. 6E). In the early stages of periodontal wound healing, the granulation tissue beneath the gingival epithelial layer consisted of *Plap-1* lineage cells and αSMA-positive myofibroblasts (Fig. 6F,G). Of the αSMA-stained cells in granulation tissue, 20.2±6.7% were Plap-1 lineage cells (n=6; mean±s.d.), which was 22.4±6.7% of the total Plap-1 lineage cells in the granulation tissue (n=6; mean±s.d.). These data suggest the partial contribution of Plap-1$^+$ cells to granulation tissue formation. On day 7, in addition to most PDLCs in repaired PDL, 56.5% of osteoblasts and cementoblasts on the surface of repaired alveolar bone and cementum were derived from Plap-1$^+$ lineage cells (Fig. 6H-J). These data confirm the long-standing concept that periodontal tissue is maintained and repaired by the PDL and emphasize the importance of the PDL.

The mural cell population in the PDL consists of quiescent cells

Long-term lineage-tracing analysis with Nes-Cre revealed that Nes$^+$ mural cells were quiescent and remained perivascular for up to a year without expansion during periodontal tissue homeostasis (Fig. S7A). Based on this observation, we performed a ligature experiment with Nes-Cre lineage tracing to determine whether *Plap-1*$^+$*Nes*$^+$ cells contribute to periodontal tissue repair (Fig. S7B). On day 7, after ligature removal, we did not detect the *Nes* lineage cells in repaired PDL, alveolar bone or cementum (Fig. S7C). These results suggest that *Nes*$^+$ mural cells in the PDL do not contribute to the periodontal tissue repair in a cell-autonomous manner.

DISCUSSION

Periodontitis is a chronic inflammation of periodontal tissues caused by bacterial biofilms, which eventually cause irreversible destruction of periodontal tissues. Periodontitis has a high prevalence worldwide and is the most common cause of tooth loss in adults in developed countries. In addition to attaching teeth to the alveolar bone, the PDL interferes with and senses the occlusal force and transmits it to the central nervous system (Beertsen et al., 1997). Dental implants, however, lack these functions because they form a direct connection to the alveolar bone (osseointegration) without the PDL. Fibrous attachment of the PDL is one of the most clinically important indicators of periodontal disease and regeneration. It has long been proposed that the PDL contains stem/progenitor populations based on the fact that periodontal tissue can partially regenerate (Kitamura et al., 2016; Sallum et al., 2019) and has a large adaptive capacity for orthodontic treatment and occlusal forces in addition to remodeling capacity (Beertsen et al., 1997). PDL tissue attached to extracted human teeth has been analyzed extensively, and PDL stem cells (PDLSCs) with minimal stemness criteria (Mao et al., 2012), including *in vitro* differentiation capacity to osteoblasts and ectopic bone formation by transplantation assays, have been widely used (Li et al., 2021). However, as with MSCs in other tissues, the definition of PDLSCs is ambiguous, and rigorous *in vivo* analyses are required to define these cell types. In this study, we established a PDL single-cell atlas and demonstrated that the PDL comprises heterogeneous cell types. Notably, the stromal compartment was collectively divided into *Plap-1*$^+$ fibroblastic cells or *Ibsp*$^+$ osteo-/cementoblastic cells in a mutually exclusive manner. PLAP-1 is also highly expressed in the human PDL and used as a cultured PDLC marker (Yamada et al., 2001; Loo-Kirana et al., 2021; Mun et al., 2022). RNA velocity analysis indicated that cluster 9, *Plap-1*^{high}, with a positive velocity of *Plap-1* mRNA, constituted a potential cellular source of other PDL clusters. This population expressed *Ly6a*, the protein product of which is known to be expressed in the stem cell population and in epithelial and endothelial cells. This *Plap-1*^{high} *Ly6a*$^+$ population could be PDLSCs that maintain and repair the entire periodontal tissue and overlap with the recently defined skeletal stem cell-like population in periodontal tissue (Liang et al., 2022). To clarify the cell fate of the putative PDLSC *in vivo*, a definitive single marker gene or an intersectional lineage-tracing approach will be needed in future studies.

In this study, we also harnessed single-cell analysis in combination with Nes-GFP and Nes-Cre transgenic mice to demonstrate the presence of strictly defined mural cells in the PDL for the first time. Although the association of pericytes with MSCs in other tissues has been described (Soliman et al., 2021), our findings suggest that *Nes*$^+$ cells are quiescent mural cells near capillaries, and they did not directly contribute to PDL regeneration. Further study is needed to clarify whether they have an indirect contribution, including the release of paracrine signals and exosomes (Wagoner and Zhao, 2021). Our single-cell analysis revealed the presence of mesenchymal cells and many immune cells, especially macrophages and monocytes, in the PDL. The presence of CD45-positive immune cells has been reported (Soliman et al., 2021), but this remains inconclusive owing to the lack of efficient methods to isolate PDLCs and other cells from the PDL. Future studies should elucidate how pericytes and PDLCs repair tissues by interacting with immune cells at each stage of wound healing. Other cell types, such as plasma cells, which were not analyzed in this study (Fig. S4C), might be identified by specific isolation of immune cells and deeper sequencing.

Regeneration of the cementum-PDL-alveolar bone complex is a major goal of periodontal therapy. In contrast to bone regeneration, the mechanism of cementum regeneration remains unclear. Without regeneration of the cementum, new attachment formation by the PDL cannot be obtained even if the bone has regenerated. In the ligature model, *Ibsp*$^+$ cementoblasts disappeared from the root surface of destroyed periodontal tissue. *In vivo* lineage tracing of PDLCs demonstrated that *Ibsp*$^+$ cells reappeared in the regenerated tissue and more than half of *Ibsp*$^+$ cells originated from the PDLCs (Fig. 6H-J). However, the exact cellular dynamics of the cementoblasts remain to be investigated with definitive markers. Recent analyses of cementum development in mice have highlighted several molecules that are specifically expressed in cementoblasts (Nagata et al., 2021). In this study, we defined cementoblasts as *Plap-1*$^-$*Ibsp*$^+$*Sparcl1*$^+$ and alveolar osteoblasts as *Plap-1*$^-$*Ibsp*$^+$*Col11a1*$^+$. Sparcl1 is an ECM protein related to Sparc and is secreted by nerves and blood vessels (Naschberger et al., 2016; Fan et al., 2021). In the future, single-cell epigenetic profiling of periodontal tissue may be harnessed to identify transcriptional regulators of cementoblasts.

In conclusion, our work identified *Plap-1* as a PDLC-specific molecule, and cell-lineage analysis using knock-in mice confirmed

Development (2022) 149, dev201203. doi:10.1242/dev.201203

that PDLCs differentiate into osteoblasts and cementoblasts and play a role in periodontal tissue homeostasis. In addition, we developed a novel cell isolation method and performed scRNA-seq to generate a PDL single-cell atlas that clearly defined osteoblasts and cementoblasts. Furthermore, lineage tracing revealed that injured periodontal tissues were repaired by PDLCs. These findings will contribute to the development of efficient regenerative therapy for periodontitis.

MATERIALS AND METHODS

Mice

All animal experiments in this study were approved by the Animal Experimentation Committee of Osaka University Graduate School of Dentistry (approval numbers: R-02-012-0 and 31-001-0). *Plap-1-GFP-2A-CreER* mice were generated using a conventional gene-targeting strategy. *R26-LSL-tdTomato* (stock #007909) and *Nes-Cre* (stock #003771) were obtained from The Jackson Laboratory. *Nes-GFP* mice were provided by Dr Grigori Enikolopov of Stony Brook University, NY, USA. *Col1a1-GFP* mice were provided by Dr David Brenner, University of California, CA, USA. PCR genotyping was performed using the primers listed in Table S1. Mice were provided sterile food and water under specific pathogen-free conditions. All animal experiments complied with ARRIVE guidelines.

Embryonic stem cell targeting and vector design

A targeting vector harboring the PGK-DTA-long homology arm-GFP-2A-CreER-WPRE-pA-short homology arm sequence was generated. Correctly targeted embryonic stem cell clones were identified by PCR and confirmed by Southern blotting using the primers and probes listed in Table S1. Chimeric males were generated using standard aggregation of clumped embryonic stem cells with eight-cell embryos and transplantation procedures and were used to establish germline transmission.

Preparation of paraffin and frozen sections

Mice mice were euthanized with CO_2 gas, perfused and fixed with 4% paraformaldehyde/phosphate buffer (PFA; Fujifilm Wako Pure Chemicals, 163-20145). Maxillary bones and other tissues were harvested and, after overnight immersion fixation in PFA, the hard tissue was demineralized in demineralizing solution B (Fujifilm Wako Pure Chemicals, #041-22031) for 3-5 days with three exchanges of solution. For paraffin sections, the tissue was embedded in paraffin and sectioned at 7 µm. Hematoxylin & Eosin (HE) staining was performed as previously described (Ueda et al., 2021). For frozen sections, the tissue was immersed in 20% sucrose (Fujifilm Wako Pure Chemicals, #196-00015) solution and then embedded in TissueTech O.C.T. compound (Sakura Finetech Japan, 4583), frozen in ethanol cooled on dry ice. Tissue sectioning at 14 µm was performed using a cryostat CM3050S (Leica Microsystems). A cryofilm [type 2C(9), Section-lab, Hiroshima, Japan] was used as section support.

Fluorescence immunohistochemistry

The prepared frozen sections were washed with PBS and blocked with Blocking One Histo (Nacalai Tesque, 06349-64) for 30 min at room temperature. Sections were incubated with rabbit anti-mouse laminin polyclonal primary antibody (1:1000, Sigma-Aldrich, L9393) at 4°C overnight followed by incubation with Alexa Fluor 647-conjugated goat anti-rabbit IgG secondary antibody (1:200, Thermo Fisher Scientific, A32733) at room temperature for 30 min. For myofibroblast identification, sections were incubated with Alexa Fluor 647-conjugated anti-mouse αSMA monoclonal antibody (1:100, clone 1A4, Santa Cruz Biotechnology, sc-32251) at 4°C overnight. Nuclear and vascular staining was performed with DAPI (1:50,000, Sigma-Aldrich, D9542) and Alexa Fluor 647-conjugated Isolectin GS-IB4 (1:200, Thermo Fisher Scientific, I32450), respectively. Fluorescently labeled tissue sections were imaged using a fluorescence microscope (ECLIPSE Ti, Nikon) or Leica TCS SP8 confocal microscope (Leica Microsystems). For confocal microscopy, 10-14 *z*-stack images (total thickness of approximately 5 µm) were acquired, and 3D images were obtained using the maximum value projection method.

RNAscope fluorescence *in situ* hybridization

Cryosections were hydrated and hybridized (Advanced Cell Diagnostics) using the Multiplex Fluorescent Reagent v2 kit according to the manufacturer's instructions. Nuclei were counterstained with DAPI (1:50,000, Sigma-Aldrich, D9542), sealed with ProLong Diamond Antifade Mountant (Thermo Fisher Scientific, P36961), and observed under a Leica TCS SP8 confocal microscope, as described above. The probes used in this study are listed in Table S1.

Tamoxifen treatment

Tamoxifen (Sigma-Aldrich, T5648) was dissolved in corn oil at a concentration of 20 mg/ml and mixed overnight. Mice (6-8 weeks old) received an intraperitoneal injection of 100 µl of tamoxifen (2 mg). In low-dose experiments, 10 µl of tamoxifen (0.2 mg) was administered intraperitoneally and analyzed after 16 days. To detect any leaky expression of tdTomato, 14-week-old *Plap-1-GFP-2A-CreER; Rosa26-tdTomato* mice without tamoxifen treatment were used.

Ligature-induced periodontitis model

To induce experimental periodontitis, a 5-0 silk ligature was tied around the left maxillary second molar of 8-week-old mice as described previously (Ueda et al., 2021). After 7 days, the ligature was removed. Tissue recovery was analyzed on day 7 after removal. The contralateral molar tooth in each mouse was left unligated as intact periodontal tissue.

Isolation of PDL-derived cells

After euthanization with CO_2 gas, 8- to 12-week-old mice were perfused with PBS, and the maxilla and mandible were separated. Gingival tissue was peeled and carefully removed. Subsequently, the molars were extracted and collected into PBS in a 12-well plate. These procedures were performed under a Leica S6 stereomicroscope (Leica Microsystems). The teeth were washed three times and transferred to fresh wells. Liberase (Merck, 05401119001) or collagenase type II (Worthington Biochemical Corporation, CLS-2) solution was used to digest PDL, as described in the Results section. Liberase powder was reconstituted with 2 ml of distilled water and stored at −20°C. The working solution was prepared in digestion buffer (PBS containing 2% fetal calf serum) at a final concentration of 2 Wünsch units/ml. The teeth were then incubated in 2 ml digestion buffer in 15 ml low-binding tubes (STEMFULL; Sumitomo Bakelite, MS-90150) for 20 min at 37°C with shaking at 200 rpm. Subsequently, 20 µl of 500 mM EDTA was added, and the teeth were further incubated for 10 min at 37°C and 200 rpm. After digestion, 10 ml of buffer was added, and cells were centrifuged at 400 ***g*** for 8 min at 4°C. The pellet was resuspended in 2 ml of buffer and passed through a 70-µm cell strainer (BMS, BC-AMS-17001). After centrifugation at 320 ***g*** for 5 min at 4°C, cells were finally resuspended in 400 µl of buffer and subjected to downstream analyses. In some experiments, PDL was scraped from the surface of the mesial root of the first molar using micro-instruments, including a micro-curette (0.5 mm) (Fine Science Tools). Scraped tissue was digested as described above.

Flow cytometry analysis

The isolated cells were resuspended in FACS buffer (PBS containing 5% fetal bovine serum). The cell pellet was incubated for 30 min on ice with fluorescent protein-conjugated antibodies (Table S1). Flow cytometry analysis was performed on a FACSCanto II (BD) flow cytometer using FCS Express 7 (De Novo Software) or FlowJo v10.8 (BD Biosciences) software.

Sorting and primary culture of PDL-derived cells

Cell sorting was performed using an SH800Z Cell Sorter (Sony Biotechnology) with 100-µm microfluidic sorting chips. The isolated cells were expanded and maintained at 37°C, 5% O_2 and 10% CO_2 with a MesenCult Expansion Kit (STEMCELL Technologies, ST-05513) according to the manufacturer's protocol. The culture medium contained MesenPure, L-glutamine (Wako, 073-05391), and penicillin-streptomycin (Wako, 168-23191). For the CFU-F assay, 500-1000 sorted cells were maintained in a 6-well plate. On day 14, the cells were fixed with 100% methanol and stained with Giemsa staining solution (Nacalai Tesque,

Development (2022) 149, dev201203. doi:10.1242/dev.201203

37114-64). Fibroblastic colonies with more than 20 cells were quantified as CFU-F.

Osteogenic differentiation culture

To induce osteogenic differentiation, confluent cells were cultured in osteogenic medium comprising cell culture medium supplemented with 50 µg/ml l-ascorbic acid phosphate magnesium salt n-hydrate (Fujifilm Wako Pure Chemical, 013-19641) and 10 mM glycerol 2-phosphate disodium salt n-hydrate (Fujifilm Wako Pure Chemical, 193-02041). The medium was replaced with fresh medium every 3 days. For mineral staining, cells were fixed with cold 100% ethanol for 5 min and stained with 1.0% Alizarin Red S solution (pH adjusted to 6.4; Wako Pure Chemical Industries).

scRNA-seq

scRNA-seq was performed based on a previous report (Picelli et al., 2013; Ho et al., 2021) with the following modifications. Primer mix composed of 5 µl of lysis buffer comprising 3.1375 µl of Buffer EB (QIAGEN, 19086), 0.5 µl of 10 mM dNTP (GenScript, C01582), 0.05 µl of Phusion HF buffer [New England BioLabs (NEB), B0518S], 0.3125 µl of Proteinase K (Nacalai Tesque, 15679-64) and 1 µl of 1 µM barcoded oligo-dT primer (5′-ACGACGCTCTTCCGATCT[Barcode]NNNNNNNNTTTTTTTTTTT-TTTTTTTTTTTTTTTTTTTVN-3′, where ‘N’ is any base and ‘V’ is either ‘A’, ‘C’ or ‘G’; IDT) was aliquoted into 384-well plates. The isolated PDL-derived cells were stained with SYTOX™ Blue dead cell stain (Thermo Fisher Scientific, S34857). Unstained cells were considered live cells. Live cells were sorted into plates using a BD FACSAria III instrument (BD Biosciences; 100-µm chip) in single-cell purity mode. The plates were immediately centrifuged (500 ***g*** for 5 s at room temperature) and frozen at −80°C. Plates were incubated at 50°C for 10 min and then at 80°C for 10 min. A volume of 5 µl of first-strand reaction mix containing 2 µl of 5× Superscript IV First-Strand Buffer (Thermo Fisher Scientific, 18090050B), 0.5 µl of 100 mM DTT (Thermo Fisher Scientific), 0.0125 µl of SuperScript IV reverse transcriptase (200 U/µl, Thermo Fisher Scientific, 18090200), 0.05 µl of SUPERase In RNase Inhibitor (Thermo Fisher Scientific, AM2696) and 2.4375 µl of water was aliquoted into each well. The plates were then incubated at 55°C for 10 min, and the reaction was inactivated by incubation at 80°C for 10 min. To remove unincorporated oligos, 2 µl of exonuclease I mix containing 0.0625 µl of exonuclease I (Thermo Fisher Scientific, EN0582), 1.2 µl of 10× reaction buffer and 0.7375 µl of water was added, and the mixture was incubated at 37°C for 20 min. Samples were pooled and purified using a DNA Clean & Concentrator Kit-100 (Zymo Research, D4030), concentrated using a DNA Clean & Concentrator Kit-5 (Zymo Research, D4014), and eluted in 12 µl of Buffer EB. Eluted cDNA was denatured at 95°C for 2 min and immediately placed on ice for 2 min. The cDNA was pre-amplified using the Accel-NGS 1S Plus DNA Library Kit (10096; Swift Biosciences). A volume of 10 µl of Adaptase reaction mix containing 1.25 µl of Buffer EB, 2 µl of Buffer G1, 2 µl of Reagent G2, 1.25 µl of Reagent G3, 0.5 of µl Enzyme G4, 0.5 µl of Enzyme G5 and 0.5 µl of Enzyme G6 was added, and the mixture was incubated at 37°C for 15 min and at 95°C for 2 min. A volume of 23.5 µl of Extension reaction mix containing 9.25 µl of Buffer EB, 1 µl of Reagent Y1, 3.5 µl of Reagent W2, 8.75 µl of Buffer W3 and 1 µl of Enzyme W4 was added, and the mixture was incubated at 98°C for 30 s, 63°C for 15 s and 68°C for 5 min. Amplified cDNA was purified using 26.1 µl of AMPure XP beads (Beckman Coulter Diagnostics, A63881) and eluted in 19.5 µl of Buffer EB. To amplify cDNA libraries, each well was mixed with 3 µl of 10 µM i5 primer (5′-AATGATACGGCGACCACCGAGATCTACAC[i5]ACACTCTTTCCCTACACGACGCTCTTCCGATCT-3′; IDT), 2.5 µl of 12 µM D7 primer (CAAGCAGAAGACGGCATACGAGATCGAGTAATGTGACTGGAGTTCAGACGTGTGCTCTTCCGATC-3′; IDT) and 25 µM KAPA HiFi ReadyMix (KAPA Biosystems, KK2602). Amplification was performed using the following program: 98°C for 3 min; 14 cycles of 98°C for 20 s, 67°C for 15 s and 72°C for 2 min; and a final hold at 72°C for 5 min. Each well was purified using 30 µl of AMPure XP beads, eluted in 30 µl of Buffer EB and transferred to a new PCR tube. Each well was then purified using 18 µl of AMPure XP beads and eluted in 10 µl of buffer EB. Amplified cDNA (1 ng) was mixed with water to a total volume of 5 µl. The following reactions were performed using the Nextera XT DNA Library Prep Kit (Illumina, FC-131-1096). Each well was mixed with 10 µl of Nextera TD buffer and 5 µl of Amplicon Tagment enzyme and then incubated at 55°C for 5 min for tagmentation. After tagmentation, samples were mixed with 20 µl of DNA Binding Buffer (Zymo Research, D4004−1-L), purified using 32 µl of AMPure XP beads and eluted in 16 µl of Buffer EB. The eluted DNA was mixed with 2 µl of 10 µM i5 primer, 2 µl of 10 µM P7 primer (5′-CAAGCAGAAGACGGCATACGAGAT[i7]GTCTCGTGGGCTCGG-3′) and 20 µM NEBNext High-Fidelity 2× PCR Master Mix (NEB, #M0541L). Amplification was performed using the following program: 72°C for 3 min, 98°C for 30 s, eight cycles of 98°C for 10 s, 66°C for 30 s and 72°C for 1 min, and a final hold at 72°C for 5 min. After amplification, the samples were purified using 32 µl of AMPure XP beads and eluted in 10 µl of Buffer EB. Purified samples were quantified for concentration using the Qubit dsDNA HS Assay Kit (Thermo Fisher Scientific, Q32854), and size was measured using a High Sensitivity D5000 Reagent Kit (Agilent Technologies, 5067-5593) and High Sensitivity D5000 Screen Tape (Agilent Technologies, 5067-5592). Sequencing libraries were sequenced on a NextSeq2000 platform (Illumina). The read length was set to 20 (read 1), eight (i7), eight (i5) and 51 (read 2) bases.

scRNA-seq data processing

BCL files were obtained from NextSeq (Illumina) and then demultiplexed and converted into FASTQ files using bcl2fastq2 (https://jp.support.illumina.com/downloads/bcl2fastq-conversion-software-v2-20.html). FASTQ reads were mapped onto mouse mm10 reference genomes using STARv2.7.6a with solo options (Dobin et al., 2013). The count tables from STAR were loaded as a Seurat object (Hao et al., 2021). Low-quality samples with extremely high (>3500) or low (<200) UMI counts or high percentages of mitochondrial genes (>10%) were removed. Downstream analyses, including normalization, scaling and clustering, were conducted using Seurat v4 functions following a standard analytic procedure. For sub-cluster analysis, stromal cells were extracted from whole cells, and normalization and scaling were performed. A phenograph was employed in the sub-cluster analysis to run more detailed clustering (Levine et al., 2015). Gene expression dynamics along pseudotime were calculated using Palantir Technologies software (Setty et al., 2019).

RNA velocity

Spliced and unspliced transcripts were quantified with velocyto (La Manno et al., 2018) using BAM files from STARv2.7.6, with the ‘–soloFeatures Gene GeneFull SJ Velocyto’ option. The output loom files were combined with the Seurat object and then converted into an h5ad file using SeuratDisk (https://mojaveazure.github.io/seurat-disk/). Further RNA velocity analyses were performed using the Scanpy (Wolf et al., 2018) and scVelo (Bergen et al., 2020) packages.

Quantification and statistical analysis

Data are presented as mean±s.d. in Figs 3F, 6J and Fig. S6D or mean±s.e.m. in Fig. 3D, Figs S3E and S4D; otherwise, raw data values were plotted. Statistical analysis was performed using GraphPad Prism v9.3 (GraphPad Software; www.graphpad.com). Statistical significance was assumed at $P<0.05$. Quantification of tdTomato, αSMA and *Ibsp* mRNA was performed by counting positive cells in the targeted area (day 3: granulation tissue upon ligature was defined as the tissue between gingival epithelium and repaired alveolar crest; day 7: PDL attached to coronal half of the root) of histological sections. One field of view each from two sections from three individual mice was used for cell quantification.

Acknowledgements

We thank Ms Kotomi Aso and Ms Minako Mori for their technical assistance. The Nes-GFP mouse line was a gift from Dr Grigori Enikolopov of Stony Brook University. The Col1a1-GFP mouse line was a gift from Dr David Brenner of the University of California, San Diego. Confocal microscopy was performed at the Center for Frontier Oral Science (Osaka University Graduate School of Dentistry). Flow cytometry was performed at the Center for Medical Research and Education (Graduate School of Medicine, Osaka University). Figures were created using Biorender.com.

Competing interests

K. Tamai is a scientific founder and received research funding from StemRIM Inc. K.M., T.K. and K.I. were employees of StemRIM, Inc. S. Murakami received research funding from StemRIM Inc.

Author contributions

Conceptualization: T.I., K. Tamai, Y.I., S.Y., L.E.O., M.T., S. Murakami; Methodology: T.I., M.I., H.S., S. Matsumoto, K. Tomita, P.B., T.S.; Validation: H.S.; Formal analysis: T.I., K.M., T.K., K.I.; Investigation: T.I., M.I., H.S., S. Matsumoto, K. Tomita, P.B., T.K., K.I.; Resources: K. Tamai, M.A.M., S.O., Y.I., S.Y.; Data curation: K.M., T.S.; Writing - original draft: T.I.; Writing - review & editing: T.I., K.M., T.K., T.S., K. Tamai, M.A.M., S.O., Y.I., S.Y., L.E.O., M.T., S. Murakami; Visualization: T.I., M.I., K.M., T.S.; Supervision: T.I., T.S., K. Tamai, Y.I., S.Y., L.E.O., M.T., S. Murakami; Project administration: T.I., K. Tamai, M.T., S. Murakami; Funding acquisition: T.I., K. Tamai, M.T., S. Murakami.

Funding

This study was supported by the Japan Society for the Promotion of Science (JSPS) KAKENHI (JP15J03981, JP16H06273, JP17K19752, JP19H03830, JP19K22713, JP19H01069 and JP22H03269).

Data availability

Single-cell RNA-sequencing data have been deposited in Gene Expression Omnibus under accession number GSE197828.

Peer review history

The peer review history is available online at https://journals.biologists.com/dev/lookup/doi/10.1242/dev.201203.reviewer-comments.pdf.

References

Abe, T. and Hajishengallis, G. (2013). Optimization of the ligature-induced periodontitis model in mice. *J. Immunol. Methods* **394**, 49-54. doi:10.1016/j.jim.2013.05.002

Awata, T., Yamada, S., Tsushima, K., Sakashita, H., Yamaba, S., Kajikawa, T., Yamashita, M., Takedachi, M., Yanagita, M., Kitamura, M., et al. (2015). PLAP-1/asporin positively regulates FGF-2 activity. *J. Dent. Res.* **94**, 1417-1424. doi:10.1177/0022034515598507

Beertsen, W., Mcculloch, C. A. G. and Sodek, J. (1997). The periodontal ligament: a unique, multifunctional connective tissue. *Periodontol. 2000* **13**, 20-40. doi:10.1111/j.1600-0757.1997.tb00094.x

Bergen, V., Lange, M., Peidli, S., Wolf, F. A. and Theis, F. J. (2020). Generalizing RNA velocity to transient cell states through dynamical modeling. *Nat. Biotechnol.* **38**, 1408-1414. doi:10.1038/s41587-020-0591-3

Caetano, A. J., Yianni, V., Volponi, A., Booth, V., D'agostino, E. M. and Sharpe, P. (2021). Defining human mesenchymal and epithelial heterogeneity in response to oral inflammatory disease. *eLife* **10**, e62810. doi:10.7554/eLife.62810

Chen, Y., Guan, Q., Han, X., Bai, D., Li, D. and Tian, Y. (2021). Proteoglycans in the periodontium: a review with emphasis on specific distributions, functions, and potential applications. *J. Periodontal. Res.* **56**, 617-632. doi:10.1111/jre.12847

De Jong, T., Bakker, A. D., Everts, V. and Smit, T. H. (2017). The intricate anatomy of the periodontal ligament and its development: lessons for periodontal regeneration. *J. Periodontal. Res.* **52**, 965-974. doi:10.1111/jre.12477

Dobin, A., Davis, C. A., Schlesinger, F., Drenkow, J., Zaleski, C., Jha, S., Batut, P., Chaisson, M. and Gingeras, T. R. (2013). STAR: ultrafast universal RNA-seq aligner. *Bioinformatics* **29**, 15-21. doi:10.1093/bioinformatics/bts635

Fan, S., Gangwar, S. P., Machius, M. and Rudenko, G. (2021). Interplay between hevin, SPARC, and MDGAs: modulators of neurexin-neuroligin transsynaptic bridges. *Structure* **29**, 664-678.e6. doi:10.1016/j.str.2021.01.003

Foster, B. L., Ao, M., Salmon, C. R., Chavez, M. B., Kolli, T. N., Tran, A. B., Chu, E. Y., Kantovitz, K. R., Yadav, M., Narisawa, S. et al. (2018). Osteopontin regulates dentin and alveolar bone development and mineralization. *Bone* **107**, 196-207. doi:10.1016/j.bone.2017.12.004

Hao, Y., Hao, S., Andersen-Nissen, E., Mauck, W. M., Zheng, S., Butler, A., Lee, M. J., Wilk, A. J., Darby, C., Zager, M. et al. (2021). Integrated analysis of multimodal single-cell data. *Cell* **184**, 3573-3587.e29. doi:10.1016/j.cell.2021.04.048

Ho, Y.-T., Shimbo, T., Wijaya, E., Kitayama, T., Takaki, S., Ikegami, K., Miyashita, K., Ouchi, Y., Takaki, E., Yamamoto, R. et al. (2021). Longitudinal single-cell transcriptomics reveals a role for Serpina3n-mediated resolution of inflammation in a mouse colitis model. *Cell. Mol. Gastroenterol. Hepatol.* **12**, 547-566. doi:10.1016/j.jcmgh.2021.04.004

Horiuchi, K., Amizuka, N., Takeshita, S., Takamatsu, H., Katsuura, M., Ozawa, H., Toyama, Y., Bonewald, L. F. and Kudo, A. (1999). Identification and characterization of a novel protein, periostin, with restricted expression to periosteum and periodontal ligament and increased expression by transforming growth factor beta. *J. Bone Miner. Res.* **14**, 1239-1249. doi:10.1359/jbmr.1999.14.7.1239

Houlihan, D. D., mabuchi, Y., Morikawa, S., Niibe, K., Araki, D., Suzuki, S., Okano, H. and Matsuzaki, Y. (2012). Isolation of mouse mesenchymal stem cells on the basis of expression of Sca-1 and PDGFR-α. *Nat. Protoc.* **7**, 2103-2111. doi:10.1038/nprot.2012.125

Iwayama, T., Steele, C., Yao, L., Dozmorov, M. G., Karamichos, D., Wren, J. D. and Olson, L. E. (2015). PDGFRα signaling drives adipose tissue fibrosis by targeting progenitor cell plasticity. *Genes Dev.* **29**, 1106-1119. doi:10.1101/gad.260554.115

Iwayama, T., Sakashita, H., Takedachi, M. and Murakami, S. (2022). Periodontal tissue stem cells and mesenchymal stem cells in the periodontal ligament. *Jpn. Dental Sci. Rev.* **58**, 172-178. doi:10.1016/j.jdsr.2022.04.001

Kalamajski, S. and Oldberg, Å. (2010). The role of small leucine-rich proteoglycans in collagen fibrillogenesis. *Matrix Biol.* **29**, 248-253. doi:10.1016/j.matbio.2010.01.001

Kitamura, M., Akamatsu, M., Kawanami, M., Furuichi, Y., Fujii, T., Mori, M., Kunimatsu, K., Shimauchi, H., Ogata, Y., Yamamoto, M. et al. (2016). Randomized placebo-controlled and controlled non-inferiority phase III trials comparing trafermin, a recombinant human fibroblast growth factor 2, and enamel matrix derivative in periodontal regeneration in intrabony defects. *J. Bone Miner. Res.* **31**, 806-814. doi:10.1002/jbmr.2738

Krivanek, J., Soldatov, R. A., Kastriti, M. E., Chontorotzea, T., Herdina, A. N., Petersen, J., Szarowska, B., Landova, M., Matejova, V. K., Holla, L. I. et al. (2020). Dental cell type atlas reveals stem and differentiated cell types in mouse and human teeth. *Nat. Commun.* **11**, 4816. doi:10.1038/s41467-020-18512-7

La Manno, G., Soldatov, R., Zeisel, A., Braun, E., Hochgerner, H., Petukhov, V., Lidschreiber, K., Kastriti, M. E., Lönnerberg, P., Furlan, A. et al. (2018). RNA velocity of single cells. *Nature* **560**, 494-498. doi:10.1038/s41586-018-0414-6

Lee, J.-H., Pryce, B. A., Schweitzer, R., Ryder, M. I. and Ho, S. P. (2015). Differentiating zones at periodontal ligament-bone and periodontal ligament-cementum entheses. *J. Periodontal. Res.* **50**, 870-880. doi:10.1111/jre.12281

Levine, J. H., Simonds, E. F., Bendall, S. C., Davis, K. L., Amir, E.-D., Tadmor, M. D., Litvin, O., Fienberg, H. G., Jager, A., Zunder, E. R. et al. (2015). Data-driven phenotypic dissection of AML reveals progenitor-like cells that correlate with prognosis. *Cell* **162**, 184-197. doi:10.1016/j.cell.2015.05.047

Li, B., Ouchi, T., Cao, Y., Zhao, Z. and Men, Y. (2021). Dental-derived mesenchymal stem cells: state of the art. *Front. Cell Dev. Biol.* **9**, 654559. doi:10.3389/fcell.2021.654559

Liang, J. F., Wang, J., Ji, Y. T., Zhao, Q., Han, L. T., Miron, R. J. and Zhang, Y. F. (2022). Identification of dental stem cells similar to skeletal stem cells. *J. Dent. Res.* **101**, 1092-1100. doi:10.1177/00220345221084199

Loo-Kirana, R., Gilijamse, M., Hogervorst, J., Schoenmaker, T. and De Vries, T. J. (2021). Although anatomically micrometers apart: human periodontal ligament cells are slightly more active in bone remodeling than alveolar bone derived cells. *Front. Cell Dev. Biol.* **9**, 709408. doi:10.3389/fcell.2021.709408

Luan, X., Dangaria, S., Ito, Y., Walker, C. G., Jin, T., Schmidt, M. K., Galang, M. T. and Druzinsky, R. (2009). Neural crest lineage segregation: a blueprint for periodontal regeneration. *J. Dent. Res.* **88**, 781-791. doi:10.1177/0022034509340641

Mao, J. J., Robey, P. G. and Prockop, D. J. (2012). Stem cells in the face: tooth regeneration and beyond. *Cell Stem Cell* **11**, 291-301. doi:10.1016/j.stem.2012.08.010

Men, Y., Wang, Y., Yi, Y., Jing, D., Luo, W., Shen, B., Stenberg, W., Chai, Y., Ge, W.-P., Feng, J. Q. et al. (2020). Gli1+ periodontium stem cells are regulated by osteocytes and occlusal force. *Dev. Cell* **54**, 639-654.e6. doi:10.1016/j.devcel.2020.06.006

Méndez-Ferrer, S., Michurina, T. V., Ferraro, F., Mazloom, A. R., Macarthur, B. D., Lira, S. A., Scadden, D. T., Maâ€™Ayan, A., Enikolopov, G. N. and Frenette, P. S. (2010). Mesenchymal and haematopoietic stem cells form a unique bone marrow niche. *Nature* **466**, 829-834. doi:10.1038/nature09262

Muhl, L., Genové, G., Leptidis, S., Liu, J., He, L., Mocci, G., Sun, Y., Gustafsson, S., Buyandelger, B., Chivukula, I. V. et al. (2020). Single-cell analysis uncovers fibroblast heterogeneity and criteria for fibroblast and mural cell identification and discrimination. *Nat. Commun.* **11**, 3953. doi:10.1038/s41467-020-17740-1

Mun, S., Kim, S. M., Choi, M.-J. and Jang, Y.-J. (2022). Transcriptome profile of membrane and extracellular matrix components in ligament-fibroblastic progenitors and cementoblasts differentiated from human periodontal ligament cells. *Genes* **13**, 659. doi:10.3390/genes13040659

Nagata, M., Chu, A. K. Y., Ono, N., Welch, J. D. and Ono, W. (2021). Single-cell transcriptomic analysis reveals developmental relationships and specific markers of mouse periodontium cellular subsets. *Front. Dent. Med.* **2**, 679937. doi:10.3389/fdmed.2021.679937

Nagayasu-Tanaka, T., Anzai, J., Takaki, S., Shiraishi, N., Terashima, A., Asano, T., Nozaki, T., Kitamura, M. and Murakami, S. (2015). Action mechanism of fibroblast growth factor-2 (FGF-2) in the promotion of periodontal

regeneration in Beagle dogs. *PLoS One* **10**, e0131870. doi:10.1371/journal.pone.0131870

Naschberger, E., liebl, A., Schellerer, V. S., Schütz, M., Britzen-Laurent, N., Kölbel, P., Schaal, U., Haep, L., Regensburger, D., Wittmann, T. et al. (2016). Matricellular protein SPARCL1 regulates tumor microenvironment-dependent endothelial cell heterogeneity in colorectal carcinoma. *J. Clin. Invest.* **126**, 4187-4204. doi:10.1172/JCI78260

Naveh, G. R. S., Foster, J. E., Silva Santisteban, T. M., Yang, X. and Olsen, B. R. (2018). Nonuniformity in ligaments is a structural strategy for optimizing functionality. *Proc. Natl. Acad. Sci. USA* **115**, 9008-9013. doi:10.1073/pnas.1807324115

Pagella, P., De Vargas Roditi, L., Stadlinger, B., Moor, A. E. and Mitsiadis, T. A. (2021). A single-cell atlas of human teeth. *iScience* **24**, 102405. doi:10.1016/j.isci.2021.102405

Picelli, S., Björklund, Å. K., Faridani, O. R., Sagasser, S., Winberg, G. and Sandberg, R. (2013). Smart-seq2 for sensitive full-length transcriptome profiling in single cells. *Nat. Methods* **10**, 1096-1098. doi:10.1038/nmeth.263

Roguljic, H., Matthews, B. G., Yang, W., Cvija, H., Mina, M. and Kalajzic, I. (2013). In vivo identification of periodontal progenitor cells. *J. Dent. Res.* **92**, 709-715. doi:10.1177/0022034513493434

Sakashita, H., Yamada, S., Kinoshita, M., Kajikawa, T., Iwayama, T. and Murakami, S. (2021). Mice lacking PLAP-1/asporin counteracts high fat diet-induced metabolic disorder and alveolar bone loss by controlling adipose tissue expansion. *Sci. Rep.* **11**, 4970. doi:10.1038/s41598-021-84512-2

Sallum, E. A., Ribeiro, F. V., Ruiz, K. S. and Sallum, A. W. (2019). Experimental and clinical studies on regenerative periodontal therapy. *Periodontol. 2000* **79**, 22-55. doi:10.1111/prd.12246

Setty, M., Kiseliovas, V., Levine, J., Gayoso, A., Mazutis, L. and Pe'er, D. (2019). Characterization of cell fate probabilities in single-cell data with Palantir. *Nat. Biotechnol.* **37**, 451-460. doi:10.1038/s41587-019-0068-4

Sharpe, P. T. (2016). Dental mesenchymal stem cells. *Development* **143**, 2273-2280. doi:10.1242/dev.134189

Sodek, J. (1977). A comparison of the rates of synthesis and turnover of collagen and non-collagen proteins in adult rat periodontal tissues and skin using a microassay. *Arch. Oral Biol.* **22**, 655-665. doi:10.1016/0003-9969(77)90095-4

Soliman, H., Theret, M., Scott, W., Hill, L., Underhill, T. M., Hinz, B. and Rossi, F. M. V. (2021). Multipotent stromal cells: one name, multiple identities. *Cell Stem Cell* **28**, 1690-1707. doi:10.1016/j.stem.2021.09.001

Takimoto, A., Kawatsu, M., Yoshimoto, Y., Kawamoto, T., Seiryu, M., Takano-Yamamoto, T., Hiraki, Y. and Shukunami, C. (2015). Scleraxis and osterix antagonistically regulate tensile force-responsive remodeling of the periodontal ligament and alveolar bone. *Development* **142**, 787-796. doi:10.1242/dev.116228

Ueda, T., Iwayama, T., Tomita, K., Matsumoto, S., Iwashita, M., Bhongsatiern, P., Sakashita, H., Fujihara, C., Takedachi, M. and Murakami, S. (2021). Zbp1-positive cells are osteogenic progenitors in periodontal ligament. *Sci. Rep.* **11**, 1. doi:10.1038/s41598-021-87016-1

Wagoner, Z. W. and Zhao, W. (2021). Therapeutic implications of transplanted-cell death. *Nat. Biomed. Eng.* **5**, 379-384. doi:10.1038/s41551-021-00729-6

Wilson, K. R., Kang, I. H., Baliga, U., Xiong, Y., Chatterjee, S., Moore, E., Parthiban, B., Thyagarajan, K., Borke, J. L., Mehrotra, S. et al. (2018). Hematopoietic stem cells as a novel source of dental tissue cells. *Sci. Rep.* **8**, 8026. doi:10.1038/s41598-018-26258-y

Wolf, F. A., Angerer, P. and Theis, F. J. (2018). SCANPY: large-scale single-cell gene expression data analysis. *Genome Biol.* **19**, 15. doi:10.1186/s13059-017-1382-0

Xiong, J., Gronthos, S. and Bartold, P. M. (2013). Role of the epithelial cell rests of Malassez in the development, maintenance and regeneration of periodontal ligament tissues. *Periodontol. 2000* **63**, 217-233. doi:10.1111/prd.12023

Yamada, S., Murakami, S., Matoba, R., Ozawa, Y., Yokokoji, T., Nakahira, Y., Ikezawa, K., Takayama, S.-, Matsubara, K. and Okada, H. (2001). Expression profile of active genes in human periodontal ligament and isolation of PLAP-1, a novel SLRP family gene. *Gene* **275**, 279-286. doi:10.1016/S0378-1119(01)00683-7

Yamada, S., Ozawa, Y., Tomoeda, M., Matoba, R., Matsubara, K. and Murakami, S. (2006). Regulation of PLAP-1 expression in periodontal ligament cells. *J. Dent. Res.* **85**, 447-451. doi:10.1177/154405910608500510

Yamada, S., Tomoeda, M., Ozawa, Y., Yoneda, S., Terashima, Y., Ikezawa, K., Ikegawa, S., Saito, M., Toyosawa, S. and Murakami, S. (2007). PLAP-1/asporin, a novel negative regulator of periodontal ligament mineralization. *J. Biol. Chem.* **282**, 23070-23080. doi:10.1074/jbc.M611181200

Yuan, X., Pei, X., Zhao, Y., Tulu, U. S., Liu, B. and Helms, J. A. (2018). A Wnt-responsive PDL population effectuates extraction socket healing. *J. Dent. Res.* **97**, 803-809. doi:10.1177/0022034518755719

Zhao, J., Volponi, A. A., Caetano, A. and Sharpe, P. T. (2020). Mesenchymal stem cells in teeth. In *Encyclopedia of Bone Biology*, pp. 109-118. Elsevier.

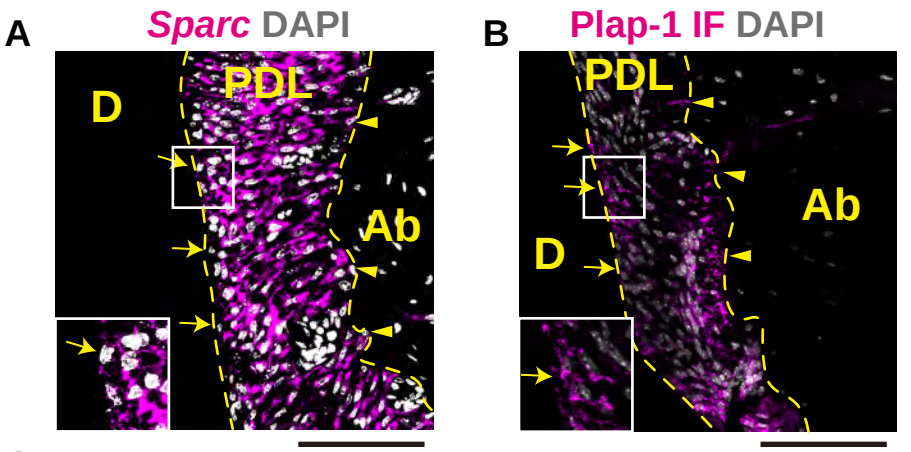

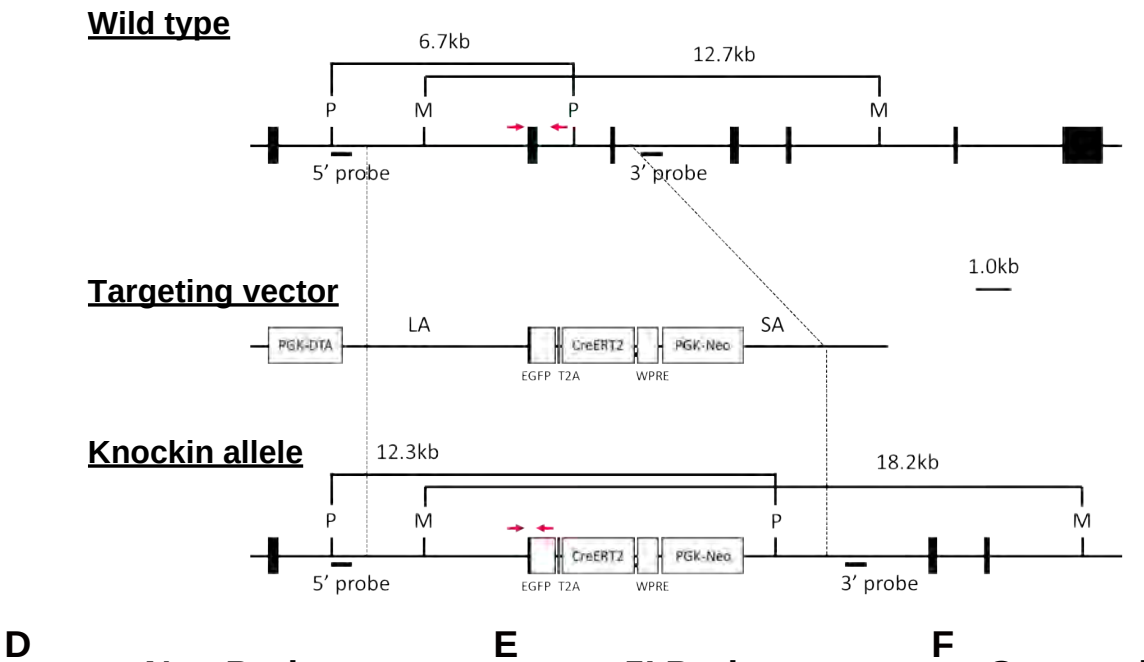

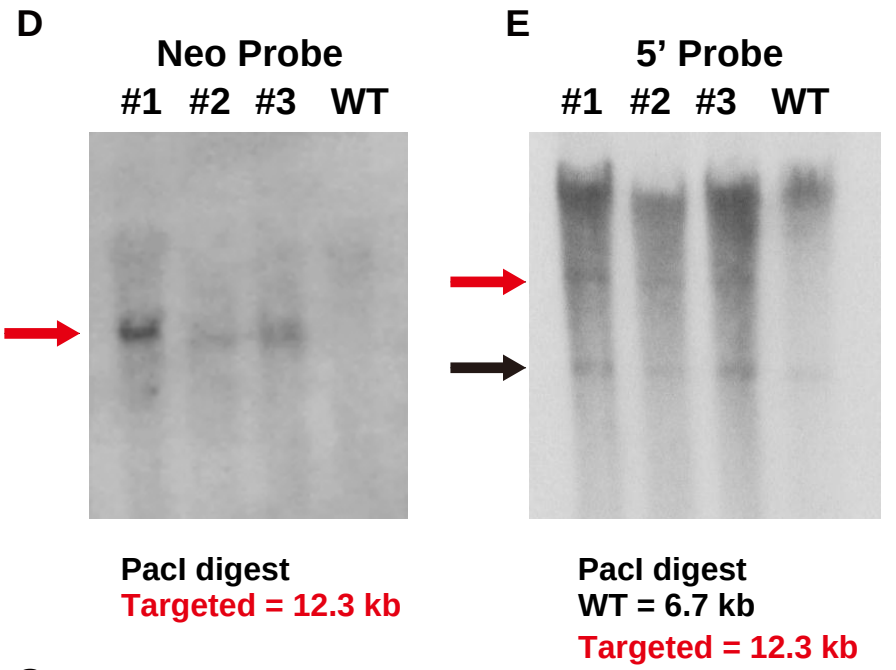

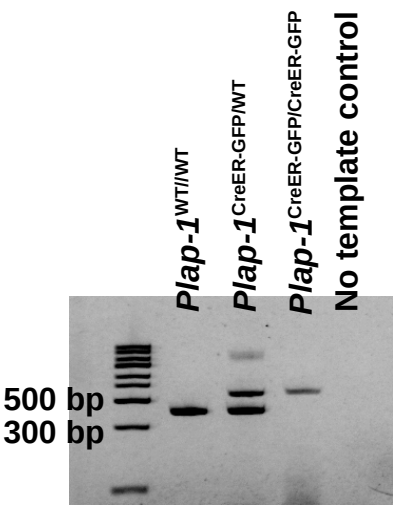

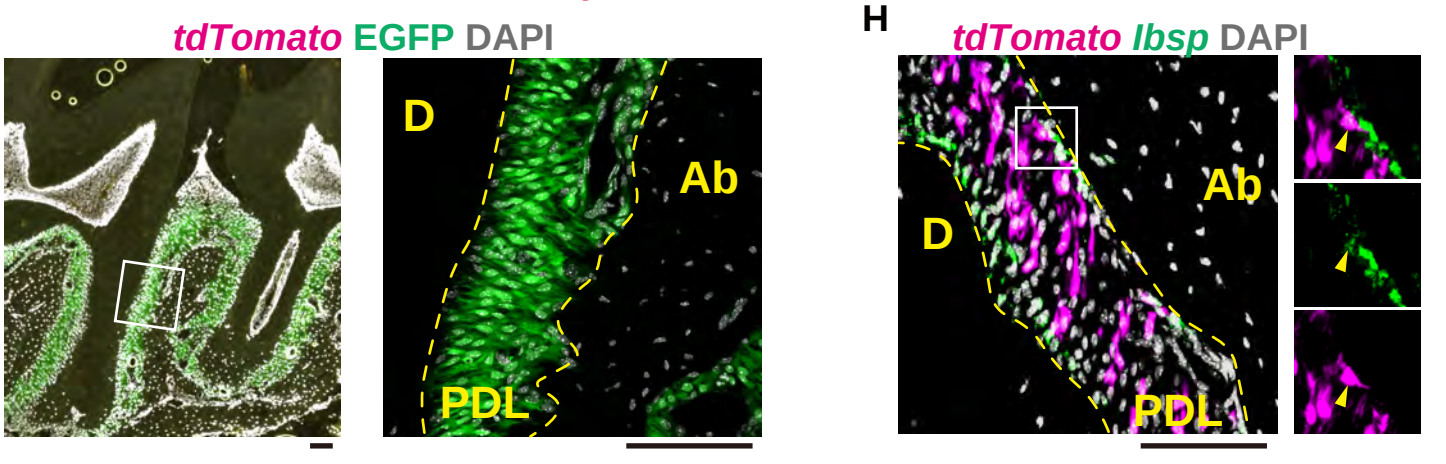

Fig. S1. Generation of Plap-1-GFP-2A-CreER knock-in mice

A. Representative *Sparc* mRNA expression in the periodontal ligament (PDL). In contrast to *Plap1*, cells on the surface of the alveolar bone and cementum expressed *Sparc*. Arrows indicate cementoblasts. Arrowheads indicate osteoblasts. All PDL images in this paper are presented in this direction (left: cementum/dentin/root, right: alveolar bone).

B. Representative Plap-1 immunofluorescent staining in the PDL. Both fibroblastic and cemento/osteoblastic cells were stained.

C. Gene targeting strategy for *Plap-1-GFP-2A-CreER* knockin mice. Structure of the mouse *Plap-1* locus (WT allele), the *Plap-1* targeting construct (Targeting vector), and the predicted mutant *Plap-1* gene (KI). Exons are represented by boxes. Exons 2 and 3 of *Plap-1* gene were replaced with the *EGFP-T2A-CreERT2-WPRE-PGK-Neo* sequence. PGK-DTA gene was attached to the 5' end of the genomic fragment for negative selection. The external homologous regions shown in the targeting allele were used as genomic probes for Southern blot analysis. Southern blot analysis for targeted clone screening was carried out using PacI (P) and MunI (M). The primer pairs for genotyping PCR are shown in the red arrow.

D. Southern blot analysis using Neo probe. The targeted (12.3 kb) band was detected using a neo probe and the PacI-digested DNA from ES cells.

E. Southern blot analysis using 5’ probe. The endogenous (6.7 kb) and targeted (12.3 kb) bands were detected using a 5’ probe and the PacI-digested DNA from ES cells.

F. Representative genotyping PCR result. The expected size of wildtype and knockin alleles are 368 bp and 564 bp, respectively.

G. Representative fluorescent images of 14-week-old *Plap-1-GFP-2A-CreER; Rosa26-tdTomato* mice without tamoxifen treatment. No leaky tdTomato expressions were detected (lower magnification in left panel, higher magnification in right panel).

H. Representative tdTomato (magenta) and *Ibsp* mRNA (green) expression in the PDL 16 days after a 1/10 dose tamoxifen treatment. A limited number of PDLC were labeled and some cells in cemento-/osteoblastic zones were double-positive for tdTomato and Ibsp. Insets show Ibsp expressing Plap-1-lineage cells.

D: Dentin, Ab: Alveolar bone, scale bars: 100 μm.

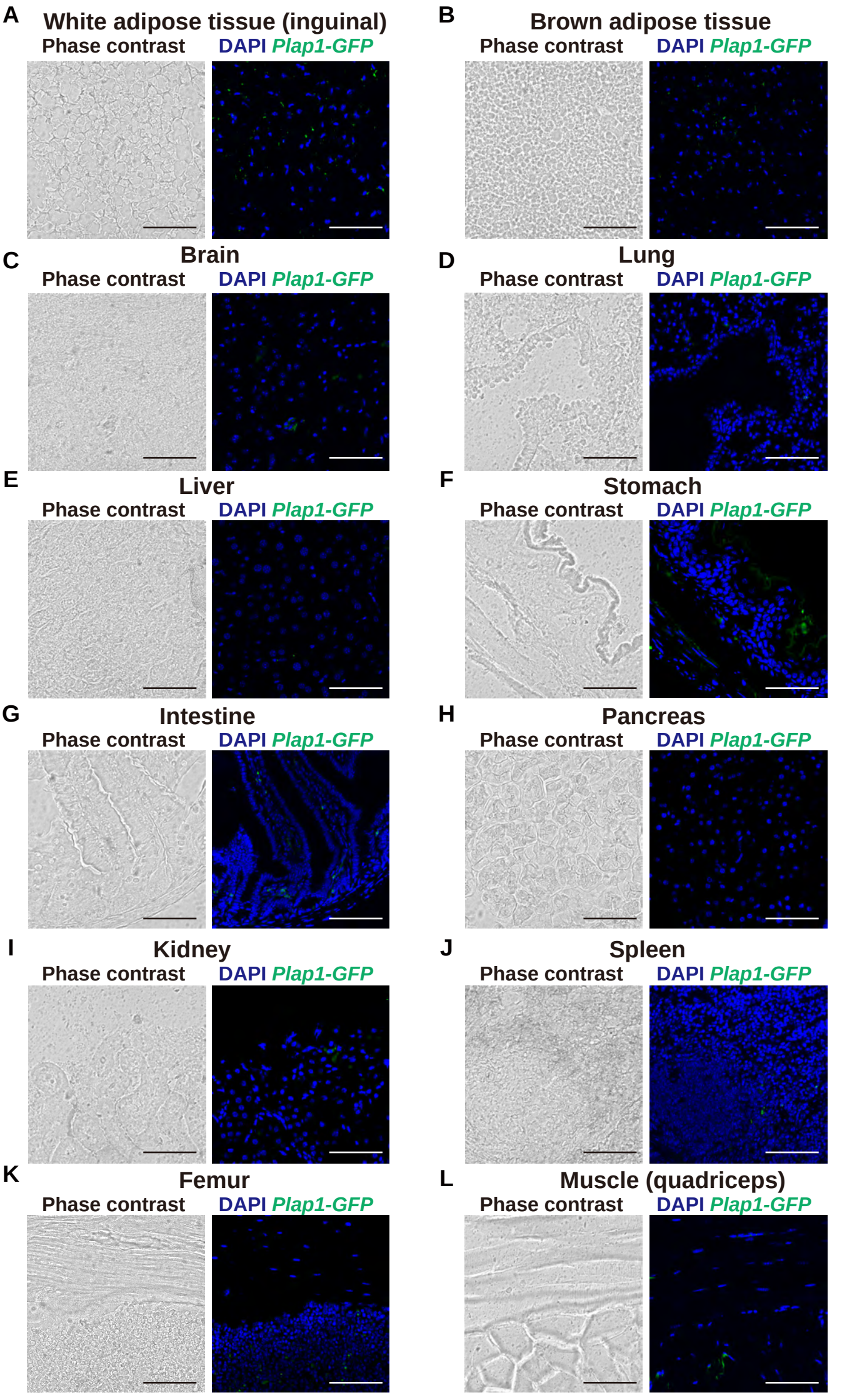

Fig. S2. Plap-1-positive cells in the tissues outside the oral cavity. Representative phase contrast and fluorescent images of inguinal white adipose tissue (A), brown adipose tissue (B), brain (C), lung(D), live (E), stomach (F), intestine (G), pancreas (H), kidney (I), spleen (J), femur including bone marrow (K), and skeletal muscle of quadriceps (L) of *Plap-1-GFP-2A-CreER* knockin mice. Scale bars: 100 μm.

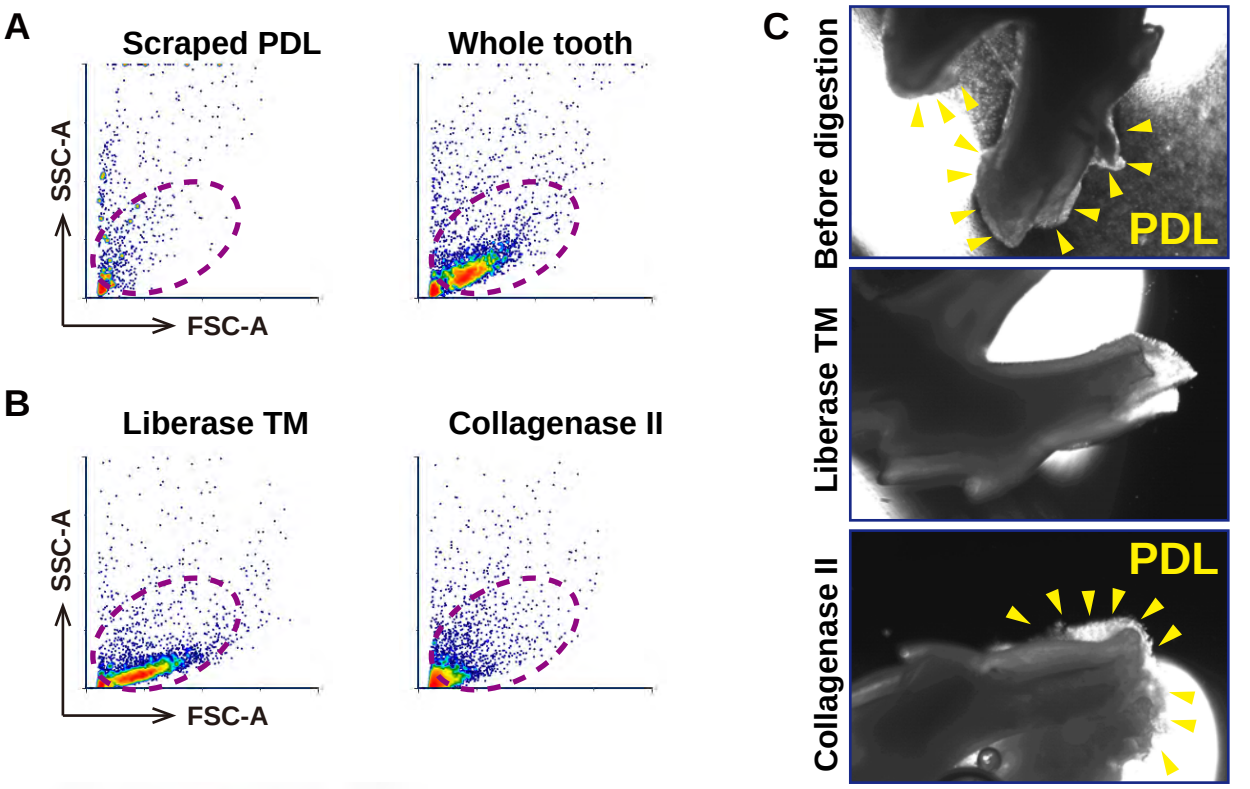

Fig. S3. Development of isolation method for PDL

A. Representative flow cytometry FSC/SSC plot for digested PDL. As a starting material, scraped PDL and whole teeth were compared.

B. Representative flow cytometry FSC/SSC plot for digested PDL. Liberase TM and collagenase II were compared.

C. Representative Microscopic images of extracted teeth before and after enzymatic digestion. Complete digestion of PDL by Liberase TM was confirmed. On the contrary, PDL remained on the root surface in collagenase II treated teeth. The yellow arrowheads showed PDL.

D. Representative HE staining image of the tooth socket after the extraction. PDL tissue remained on the alveolar bone surface, but cells in the furcation area close to the alveolar crest were mostly removed.

E. Ratio and the absolute number of live cells obtained from Liberase TM or collagenase II treatment.

F. Representative epifluorescent images of Col1a1-GFP mouse.

G. Representative flow cytometry GFP histograms from gingiva and PDL of wildtype, *Plap- 1-GFP-2A-CreER*, and *Col1a1-GFP* mice.

D: Dentin, Ab: Alveolar bone, scale bars: 100 μm.

Fig. S4

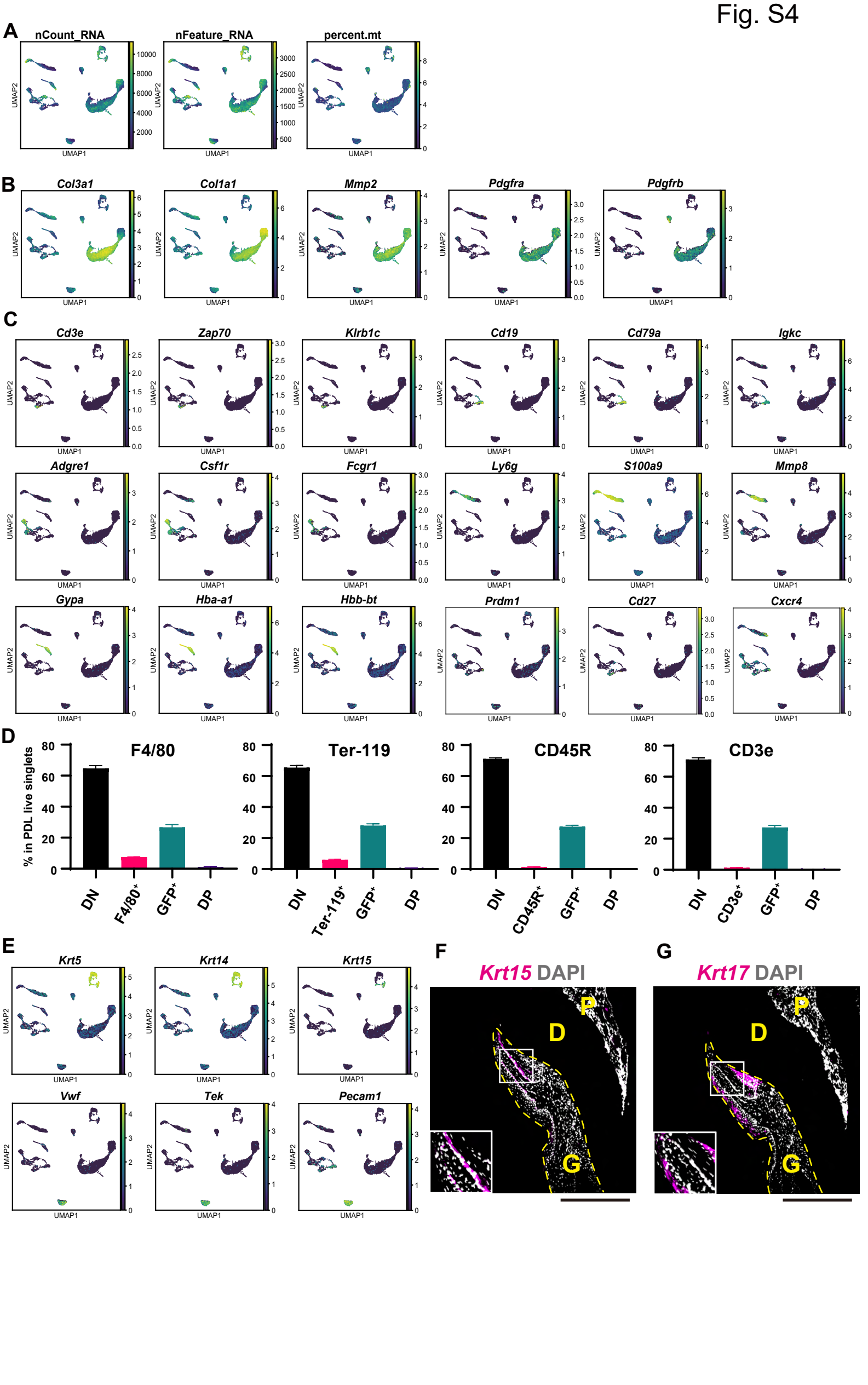

Fig. S4. Clustering analysis of non-stromal PDL-derived cells

A. UMAP plots representing UMI counts, unique gene numbers, and percentages of mitochondrial genes.

B. UMAP plots showing expressions of stromal cell marker genes.

C. UMAP plots showing expressions of immune cell marker genes.

D. Cellular composition analysis by flow cytometry. Within the PDL-enriched population, F4/80, Ter-119, CD45R, and CD3e-positive cells were quantified (n=3 mice).

E. UMAP plots showing expressions of epithelial cell marker genes.

F. Representative *Krt15* mRNA expression in the gingival epithelium. The expression was restricted to the basement membrane of the gingival epithelium.

G. Representative *Krt17* mRNA expression in the gingival epithelium. The expression was restricted to the junctional epithelium and oral epithelium.

D: Dentin, Ab: Alveolar bone, scale bars: 200 μm.

Fig. S5

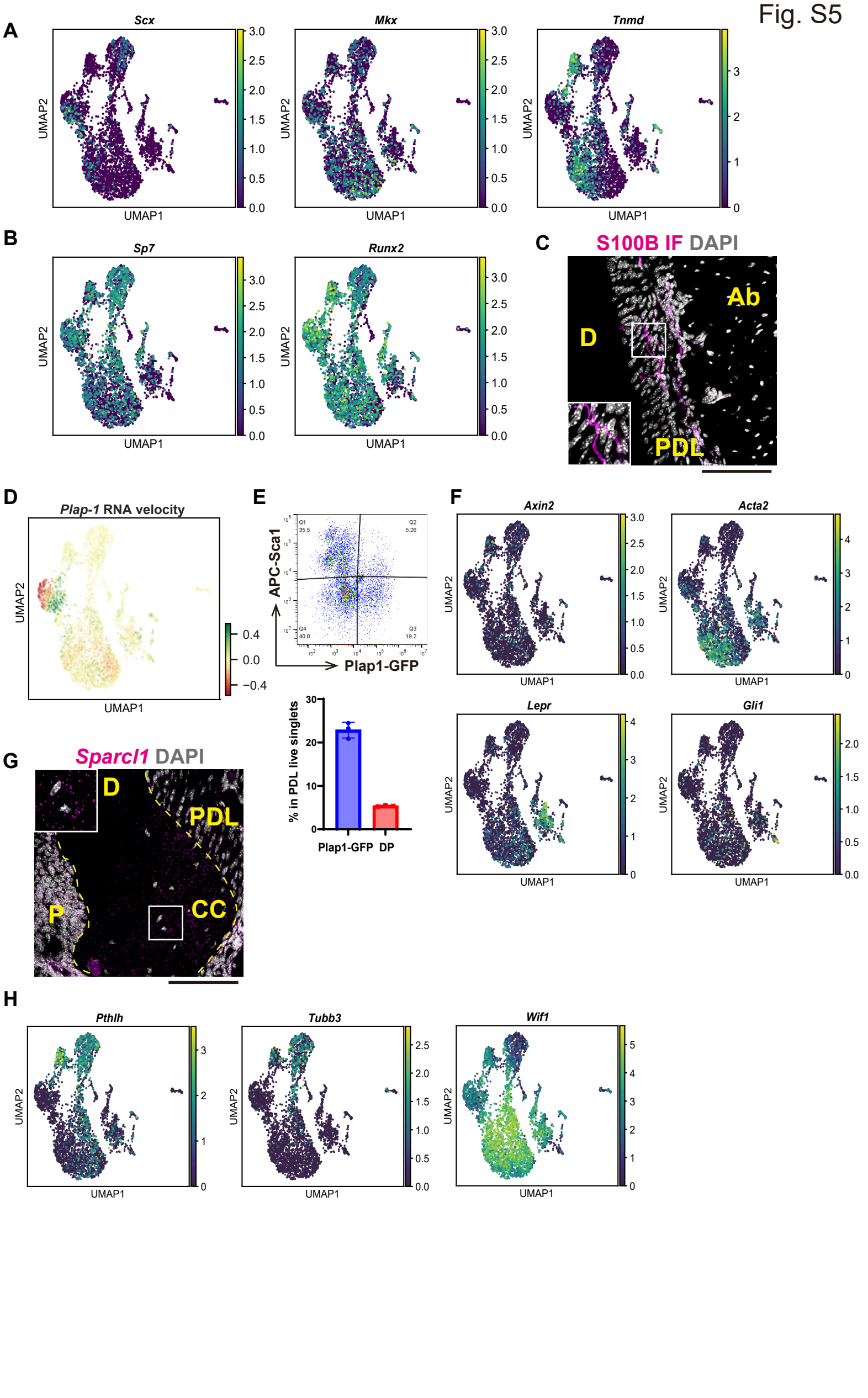

Fig. S5. Clustering analysis of stromal PDL-derived cells

A. UMAP plots showing expressions of stromal cell marker genes.

B. *Plap-1* and *Ibsp* expressions overlayed on UMAP plots.

C. Representative S100B immunofluorescent staining in the PDL.

D. *Plap-1* RNA velocity analysis overlaid on scRNA-seq UMAP plot.

E. Representative Sca-1/Plap-1-GFP plot of PDL live singlet cells (left panel). The detailed gating strategy was described in Fig. 3C. The quantification of the Plap-1-GFP (including DP) and DP cells (right panel). DP: double positive cells for Sca-1 and Plap-1-GFP.

F. UMAP plots showing expressions of putative stem cell marker genes.

G. Representative *Sparcl1* mRNA expression at root apex of the tooth. The expression was restricted to the cellular cementum.

H. Expressions of potent cementoblast marker genes on UMAP plots.

D: Dentin, Ab: Alveolar bone, P: Pulp, CC: Cellular cementum, scale bars: 100 μm.

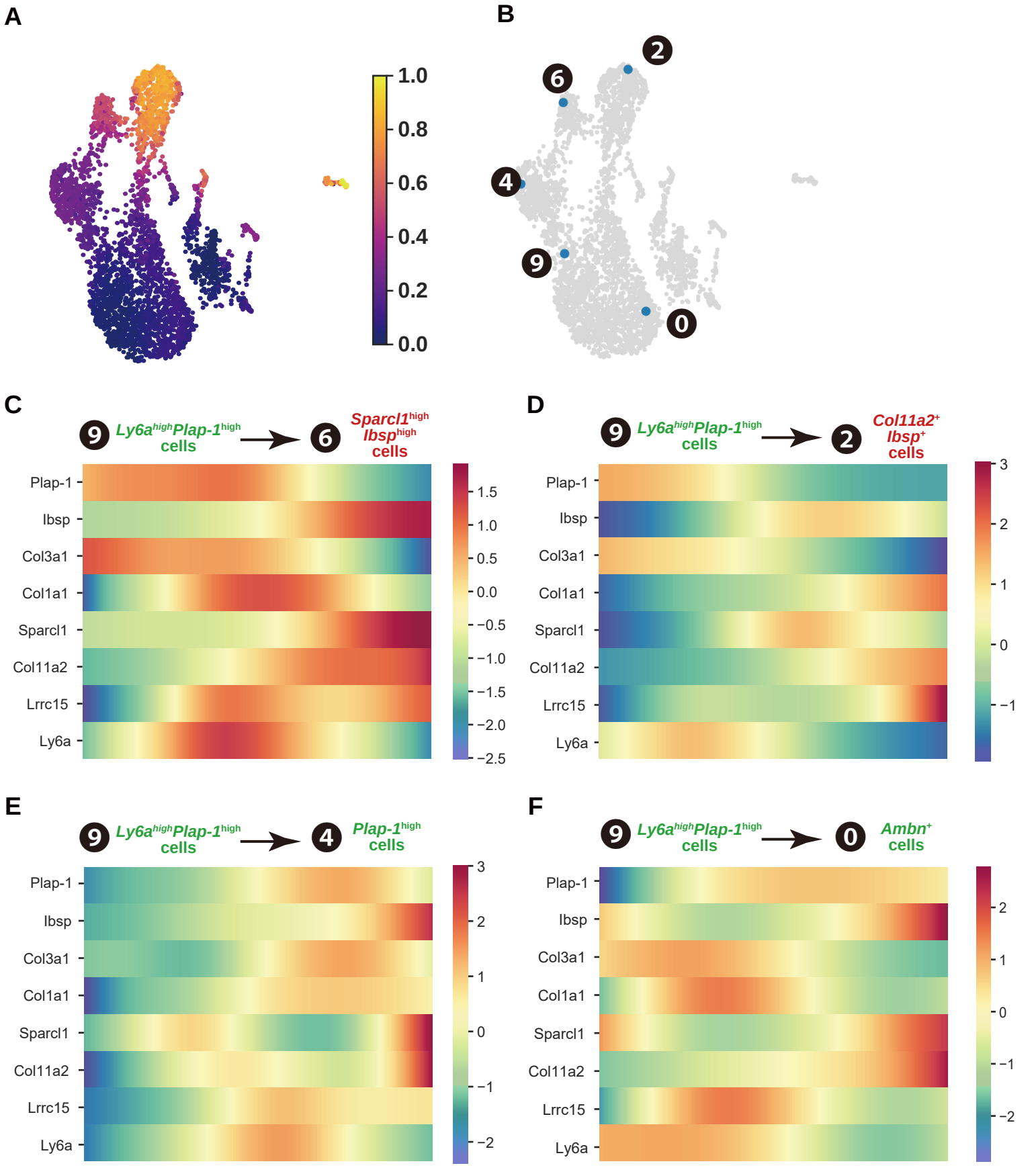

Fig. S6. Pseudotime analyses of PDLSC differentiation

A. Pseudotime analysis of stromal cells. Each dot in the UMAP plot was colored according to its pseudotime value.

B. Visualization of the cell used for following trajectory analysis in each cluster (labeled as blue). The cell in cluster 9 was designated as the root node, and others as the terminal nodes.

C-F. Heatmaps of the expression dynamics of *Plap-1*, *Ibsp*, *Col3a1*, *Col1a1*, *Sparcl1*, *Col11a2*, *Lrrc15*, and *Ly6a* through the trajectory.

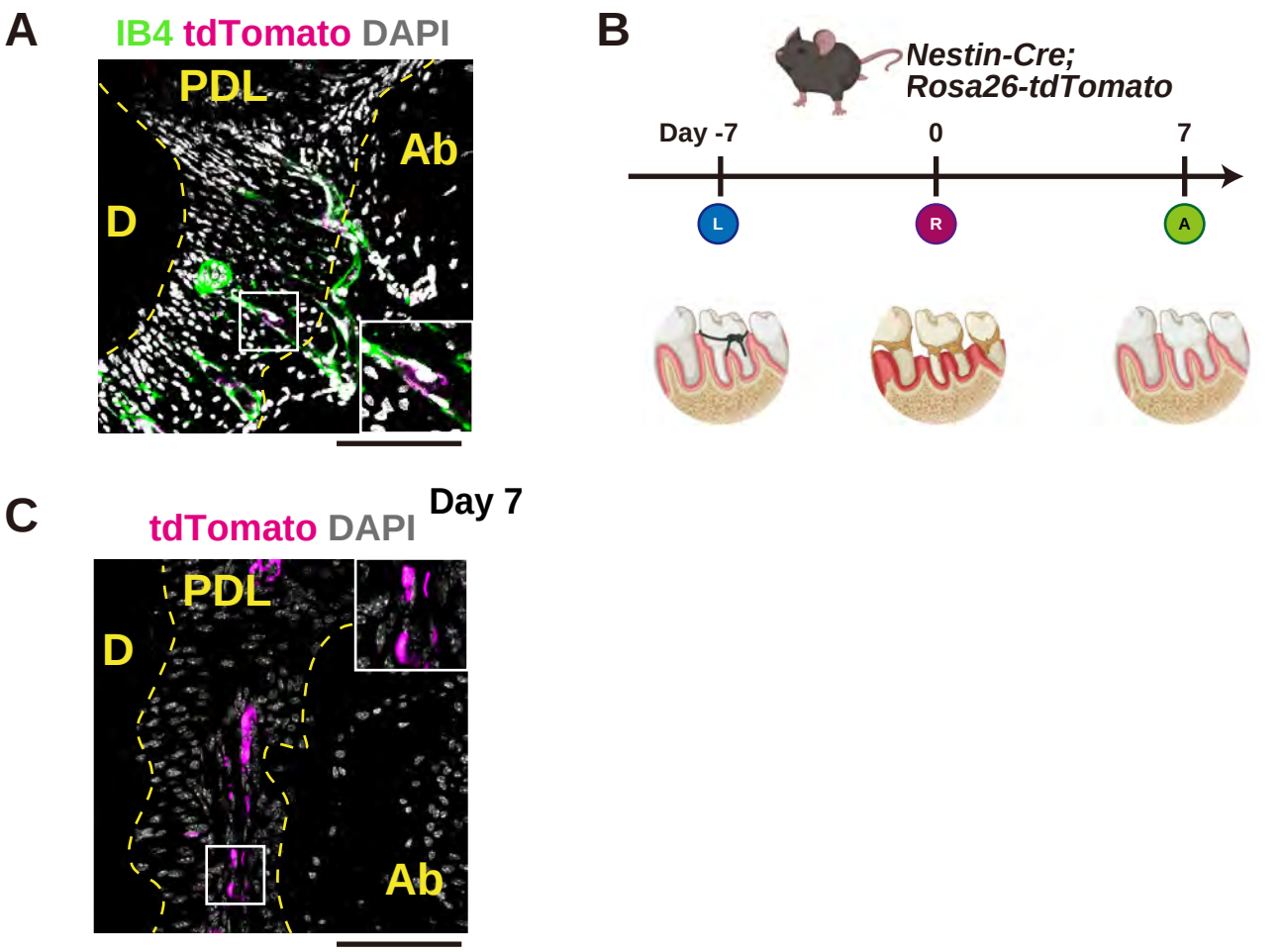

Fig. S7. Quiescent Nes^{+} mural cells in the PDL

A. Representative Nestin-lineage tracing and GS-IB-4 staining in the PDL of 1-year-old Nes-Cre; Rosa26-tdTomato mice. Nes^{+} cells remained perivascular for up to a year.

B. Overview of ligature-induced periodontitis experiments. *Nes-Cre; Rosa26-tdTomato* mice were subject to ligature placement around the second molar of the maxilla. The suture was removed 7 days after ligature placement
(designated as day 0). The repair process was analyzed on days 7. A week after suture removal, periodontal tissue was repaired. L: Ligature placement. R: removal of suture. A: Analysis of the mice.

C. Representative tdTomato expression in repaired periodontal tissue of *Nes-Cre; Rosa26-tdTomato* mice 7 days after suture removal.

D: Dentin, Ab: Alveolar bone, scale bars: 100 μm.

Table S1. Reagents used in this study

Genotyping PCR primer sequences

Plap-1-GFP-2A-CreER1	GAGGTCAAGCCTGCACTTGTA
Plap-1-GFP-2A-CreER2	GGCGGACTTGAAGAAGTCGT
Plap-1-GFP-2A-CreER3	TTCTTCAGTGCTGTGTGGGA
	Amplifying 472bp mutatnt allele, 298bp WT allele
Cre1	TCCAATTTACTGACCGTACACCAA
Cre2	CCTGATCCTGGCAATTTCGGCTA
Cre3	CTAGGCCACAGAATTGAAAGATCT
Cre4	GTAGGTGGAAATTCTAGCATCATCC
	Amplifying 540bp transgene, 324bp WT Il2 genome
R26tdTomato1	CTCTGCTGCCTCCTGGCTTCT
R26tdTomato2	CGAGGCGGATCACAAGCAATA
R26tdTomato3	TCAATGGGCGGGGGTCGTT
	Amplifying 322bp wildtype Rosa26, 243bp Rosa26-mTmG
GFP1	GCCACAAGTTCAGCGTGTCC
GFP2	GATGCCCTTCAGCTCGATGC
	Amplifying 314bp transgene

Antibodies used in flow cytometry experiments

Name	Company	Cat#	Isotype	Clone	Dilution
CD45	BioLegend	103105	PE-conjugated Rat IgG2b, κ	30-F11	1:100
CD31	BioLegend	102507	PE-conjugated Rat IgG2a, κ	MEC13.3	1:100
CD326	BioLegend	118205	PE-conjugated Rat IgG2a, κ	G8.8	1:100
CD51	BioLegend	104105	PE-conjugated Rat IgG1, κ	RMV-7	1:100
CD3e	BioLegend	100311	APC-conjugated Armenian Hamster IgG	145-2C11	1:100
CD45R/B220	BioLegend	103211	APC-conjugated Rat IgG2a, κ	RA3-6B2	1:100
F4/80	BioLegend	123115	APC-conjugated Rat IgG2a, κ	BM8	1:100
Ter-119	BioLegend	116211	APC-conjugated Rat IgG2b, κ	TER-119	1:100
Ly6a/Sca-1	BioLegend	108111	APC-conjugated Rat IgG2a, κ	D7	1:100
SYTOX AADvanced	Thermo	S10349			
SYTOX Blue	Thermo	S34857			

Antibodies used in immunofluorescent experiments

Name	Company	Cat#	Host	Dilution
Plap-1	Abcam	ab31303	Goat pAb	1:1,000
GFP	Thermo	A11122	Rabbit pAb	1:1,000
Laminin	Sigma-Aldrich	L9393	Rabbit pAb	1:1,000
Sca-1	BioLegend	108101	Rat pAb	1:1,000
S100B	Abcam	ab52642	Rabbit mAb	1:1,000

Probes used in RNAscope experiments

Gene Name	Cat #	Accession #	Target Region
Col1a1	319371	NM_007742.3	1686 - 4669
Plap-1/Aspn	502051	NM_025711.3	281 - 1315
Aspn-C2	502051-C2	NM_025711.3	281 - 1315
Bgn	455361	NM_007542.4	22 - 894
Ibsp	415501	NM_008318.3	235 - 1238
Spp1	435191	NM_001204201.1	2 - 1079
Col11a2	1077971	NM_001317722.1	112-1312
Sparcl1	424641	NM_010097.4	772 - 1909
Sparc	466781	NM_009242.5	337 - 1185
Krt15	319091	NM_008469.2	364 - 1703
Krt17	479911	NM_010663.3	3 - 1486